2019

Solvation of Isoelectronic Halide and Alkali Metal Ions by Noble Gas Atoms

Carly A. Rock
University of Mississippi

Solvation of Isoelectronic Halide and Alkali Metal Ions by Noble Gas Atoms

by

Carly A. Rock

A thesis submitted to the faculty of The University of Mississippi in partial fulfillment of the requirements of the Sally McDonnell Barksdale Honors College.

Oxford May 2019

Approved by

Advisor: Dr. Gregory S. Tschumper

Reader: Dr. Ryan C. Fortenberry

Reader: Dr. Robert J. Doerksen

Acknowledgements

I would like to thank Dr. Tschumper for allowing me to perform research within his Theoretical and Computational Quantum Chemistry Research Group during my time as an undergraduate. In addition, I would like to thank the Tschumper Research Group, especially Sarah Johnson (Arradondo), for acting as my research mentor, Dr. Thomas Sexton, Dr. Thomas Ellington, and Katelyn Dreux for their countless hours of assistance and support, and my fellow undergraduate researchers Yasmeen Abdo, Caroline Rader, and Alex Denette for all of their advice and support. I would like to thank my readers, Dr. Ryan Fortenberry and Dr. Robert Doerksen. Lastly, I would like to thank the Sally McDonnell Barksdale Honors College and the Department of Chemistry and Biochemistry for providing me with incredible opportunities and challenges throughout my time as an undergraduate at the University of Mississippi. This work was completed using computational resources from the Mississippi Center for Supercomputing Research and funding from the National Science Foundation (CHE-1338056, CHE-1664998).

Abstract

Alkali metal cations (M^+ = Li^+, Na^+, K^+, and Rb^+), as well as their corresponding isoelectronic atomic anions (X^- = H^-, F^-, Cl^-, and Br^-) were solvated with argon atoms (i.e., M^+Ar_n and X^-Ar_n where n=1−6). Full geometry optimizations were performed using the MP2 electronic structure method with a series of correlation consistent basis sets augmented with diffuse functions on argon and the anions (aug-cc-pVXZ) and weighted core valence basis sets were used for the cations (cc-pwCVXZ) that include the appropriate pseudopotentials for K^+ and Rb^+ (cc-pwCVXZ-PP). The basis sets for a particular cluster are, hereafter, simply denoted as XZ where X = T, Q, or 5. A series of single point energies and scans were also performed using MP2 and CCSD(T) methods with basis sets as large as 5Z for smaller clusters to gauge basis set and electron correlation effects. These computations were performed to explore similarities and differences between the isoelectronic cation and anion pairs (Li^+ vs. H^-, Na^+ vs. F^-, K^+ vs. Cl^-, and Rb^+ vs. Br^-).

Contents

1 Introduction

Ion solvation is an area of much interest today due to its prevalence in many areas of scientific research, such as biochemistry (i.e., specific macromolecular transport systems such as ion channels and pumps) and electrochemistry (i.e., electroplating). The most fundamental aspects of ion solvation can be probed with the formation of small clusters in which a single atomic ion is "surrounded" by a small number of isotropic, nonpolar solvent atoms such as noble gas atoms (i.e., He, Ne, Ar, etc.). As such, a vareity of experimental and computational studies have been carried out to characterize the interactions of noble gas atoms with an alkali metal or alkaline earth metal atomic cation (i.e., $M^+(Ng)_n$ or $M^{2+}(Ng)_n$).[1–21]

Over the past two decades, several theoretical investigations have been performed to specifically characterize the interactions among Li^+ and Na^+ alkali metal cations solvated with Ar atoms.[22–26] Such characterizations have led to the identification of various low energy configurations for the Li^+Ar_n and Na^+Ar_n systems. In 2004, Szymczak *et al.*[22] utilized the MP2 electronic structure method in conjunction with a triple-ζ basis set to investigate the structures and properties of the Li^+Ar_n system where n=1−6. Typical symmetric configurations (i.e., configurations defined by VSEPR Theory) were reported for low energy configurations for each cluster except Li^+Ar_5, in which the low energy configuration was reported to have an atypical, C_{4v} symmetry. More recently, Prudente *et al.*[23] reported low energy configurations for optimized Li^+Ar_n (n=2−10) clusters using the MP2 method in conjunction with a quadruple-ζ basis set. For smaller Li^+Ar_n clusters (i.e., n=1−6) the low energy configurations reported by Prudente *et al.* show good agreement with those reported by Szymczak *et al.* except for Li^+Ar_2, in which a bent configuration with C_{2v} symmetry was reported by Prudente *et al.* and a linear configuration with $D_{\infty h}$ symmetry was reported by Szymczak *et al.*

Several similar investigations have been performed to characterize the Na^+Ar_n

system, revealing some agreement among low energy configurations with the Li^+Ar_n investigations.[24–26] Two comparable investigations were performed in 2004 with aims to characterize interactions between Na^+ and Ar.[24,25] Nagata *et al.*[24] utilized the MP2 method in conjunction with a triple-ζ basis set to perform geometry optimizations on Na^+Ar_n clusters where n=1−10. Typical symmetric configurations were reported for the Na^+Ar_2 and Na^+Ar_6 clusters (i.e., $D_{\infty h}$ and O_h symmetries, respectively), whereas atypical configurations were reported for Na^+Ar_n where n=3, 4 and 5. Similarly, Giju *et al.*[25] utilized the MP2 method in conjunction with a triple-ζ basis set to identify low energy configurations for Na^+Ar_n clusters where n=1−8. In contrast to Nagata *et al.*, two low-energy configurations were reported for Na^+Ar_n clusters where n=2, 3 and 4. As seen in the previously mentioned investigation performed by Nagata *et al.*, typical and atypical configurations were identified as low energy configurations, though additional atypical configurations are reported by Giju *et al.* (i.e., C_{2v} symmetry for Na^+Ar_2 and C_{3v} symmetry for Na^+Ar_3). Additionally, a similar investigation of the Na^+Ar_n system was performed by Rhouma *et al.*[26] in 2006, in which atomistic potentials fitted to reproduce *ab initio* calculations performed at the coupled-cluster level on smaller clusters were used to investigate structures and stabilities of Na^+Ar_n (n=1−54) clusters. In comparing low energy configurations with the previous two studies, similar typical and atypical configurations were reported by Rhouma *et al.* for Na^+Ar_n clusters where n=1−8. Comparable to Giju *et al.*, two low energy configurations were reported for Na^+Ar_n clusters where n=2, 3 and 4. A slight deviation in reported symmetries appears for Na^+Ar_4, where competition takes place between the planar D_{4h} and the C_{2v} configuration rather than between the C_{2v} and T_d configuration reported by Giju *et al.*

This present study aims to build upon these prior works by using higher levels of theory (i.e., MP2 and CCSD(T) methods in conjunction with quadruple-ζ basis sets) to perform a more extensive exploration of the Li^+Ar_n and Na^+Ar_n systems, as well as to expand the exploration to include the K^+Ar_n and Rb^+Ar_n systems in order to provide a more thorough characterization of interactions between alkali metal cations and Ar atoms. Additionally, this research seeks to provide characterization of interac-

tions between halide ions and Ar atoms. Few investigations have been performed on halide ions solvated by noble gas atoms.[27–33] Moreover, to our knowledge, a systematic investigation has yet to be performed on metal cations and their corresponding isoelectronic anions. Our goal is to thoroughly describe the relationship between the structures and energetics of isoelectronic alkali metal cations and halide ions solvated with Ar atoms.

2 Computational Methods

Full geometry optimizations were performed upon the M^+Ar_n system, (where M^+=Li^+, Na^+, K^+, Rb^+ and n=1−6) and the X^-Ar_n system, (where X^-=H^-, F^-, Cl^-, Br^- and n=1−6), using the MP2 method[34] with a series of correlation consistent basis sets augmented with diffuse functions on Ar, H^-, F^-, Cl^- and Br^- (aug-cc-pVXZ)[35–37] and weighted core valence correlation consistent basis sets were used for Li^+, Na^+, K^+ and Rb^+ (cc-pwCVXZ)[38] that include the appropriate pseudopotentials for K^+ and Rb^+ (cc-pwCVXZ-PP)[39], hereafter simply denoted as XZ where X=T or Q. Single point CCSD(T)[40,41] energy computations were performed upon the MP2/QZ optimized structures with the same basis set. An additional series of single point energy computations were perfomed with the MP2 and CCSD(T) method to scan over the interatomic distances in M^+Ar_1 and X^-Ar_1 clusters using TZ and the analogous QZ and 5Z basis sets. Similarly, relaxed angular scans of M^+Ar_2 and X^-Ar_2 clusters were perfomed with the same methods and basis sets to compare electron correlation and basis set effects between the anion and cation systems.

Electronic binding energies (E_{bind}) are determined for every structure by comparing the total electronic energy of each cluster (M^+Ar_n or X^-Ar_n) to those of the isolated fragments n Ar atoms and either an M^+ or X^- ion). Similarly, the sequential binding energy for a cluster with n Ar atoms is defined by comparing its binding energy to E_{bind} for the corresponding cluster with one less Ar atom (ΔE_{bind}=$E_{bind}[M^+Ar_n]$−$E_{bind}[M^+Ar_{n-1}]$ or ΔE_{bind}=$E_{bind}[X^-Ar_n]$−$E_{bind}[X^-Ar_{n-1}]$). Note that for n=1 E_{bind}=ΔE_{bind}.

All MP2 geometry optimizations were carried out with `Gaussian16`.[42] Additionally, all single point energy computations and scans using the CCSD(T) method were performed with `Molpro2015.1`[43]. Default frozen core approximation was used for the X^-Ar_n systems, whereas for the M^+Ar_n systems frozen core was manually specified. All electrons were correlated for H^- and Li^+, whereas the 1s-like orbital was frozen

for F^- and Na^+. The 1s2s2p-like orbitals were frozen for Cl^- and the 10MDF effective core potential was utilized for K^+.[44] Similarly, the 1s2s2p3s3p-like orbitals were frozen for Br^- and the 28MDF effective core potential was utilized for Rb^+.[44] The 28MDF effective core potential for Br^-[45] was tested and compared to freezing the 1s2s2p3s3p-like orbitals which led to the decision to use frozen core approximation for Br^-. Details of this analysis can be found in the appendix.

3 Results and Discussion

All unique configurations for the M^+Ar_n and X^-Ar_n clusters identified in this study are depicted in Figures 1−4 at the MP2/QZ level of theory. Each figure shows the M^+Ar_n clusters on the left and the X^-Ar_n clusters on the right for their respective central ions and number of Ar atoms. All configurations are individually labeled with the appropriate central ion and point group. For n≥2, two low-energy minima were found for most clusters. Only one minimum was identified for Na^+Ar_6 and for Li^+Ar_n when n=2, 3, 4 and 6. The configurations reported here for the Li^+Ar_n and Na^+Ar_n clusters are consistent with those previously reported.[22,24,25]

The structures observed for these clusters include the high-symmetry fundamental geometries familiar to most chemists from VSEPR Theory[46] that effectively place the atomic ions in the center of a solvation shell of Ar atoms. As defined in Figure 5, the linear ($D_{\infty h}$ for n=1 and 2), trigonal planar (D_{3h} for n=3), tetrahedral (T_d for n=4) and octahedral (O_h for n=6) optimized structures are defined by a single bond length while the trigonal bipyramidal geometry (D_{3h} for n=5) requires only one additional bond distance. Most of the other structures are closely related distortions of these basic shapes: bent (C_{2v} for n=2), t-shaped and pyramidal (C_{2v} and C_{3v} for n=3), see-saw (C_{2v} for n=4) and square pyramidal (C_{4v} for n=5). The specification of these structures requires additional geometrical parameters (up to two unique bond lengths and two unique bond angles). The optimized geometrical parameters for each structure are reported in the Appendix. For n=6, an interesting and completely novel C_{2v} minimum has also been identified for every ion examined except Li^+ and Na^+. This C_{2v} structure appears to be derived from a pentagonal bipyramid with a vacant equatorial position in the same manner a see-saw structure is derived from a trigonal bipyramid.

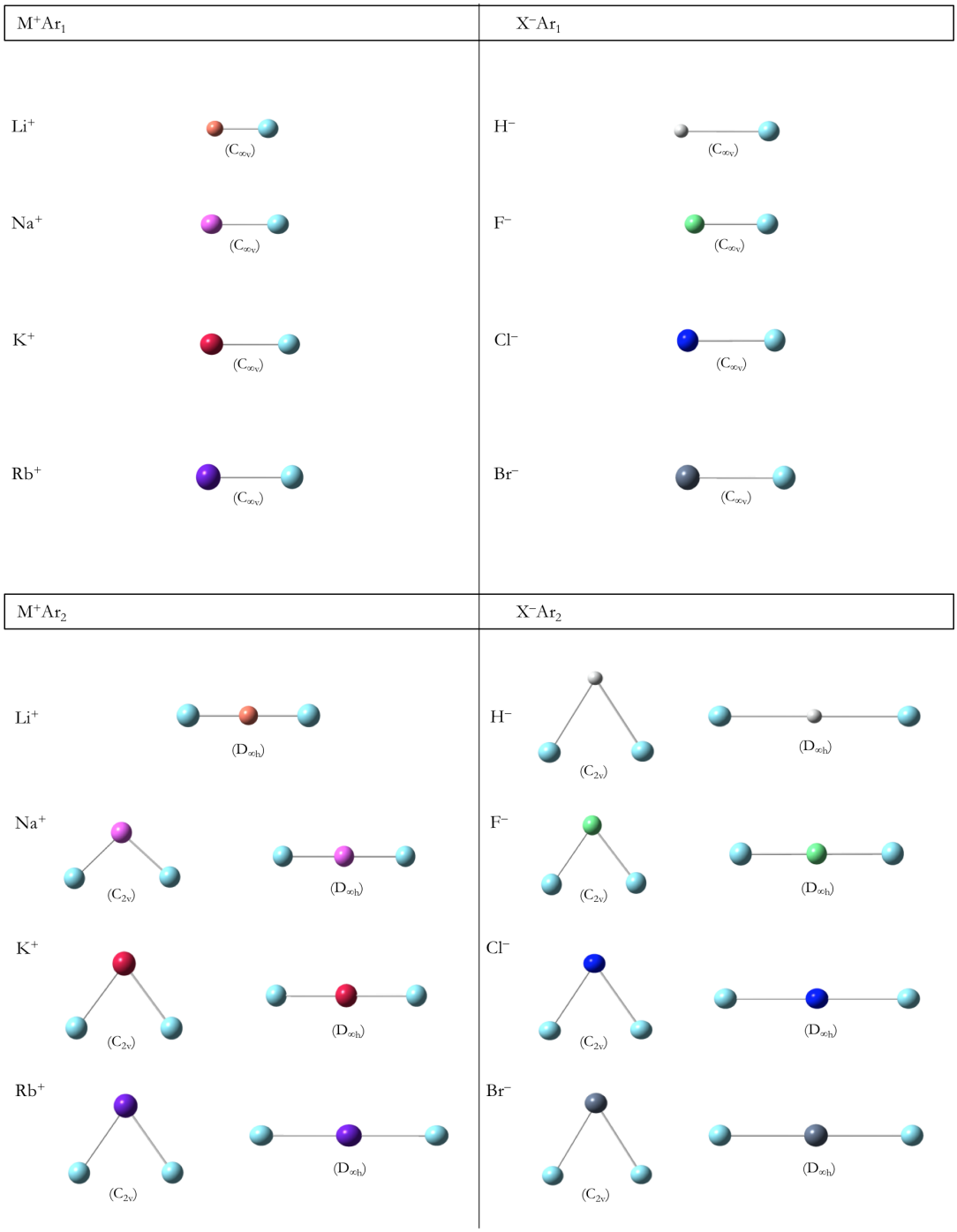

Figure 1: M^+Ar_n and X^-Ar_n clusters and their respective configurations labeled with the appropriate central ion and point group at the MP2/QZ level of theory.

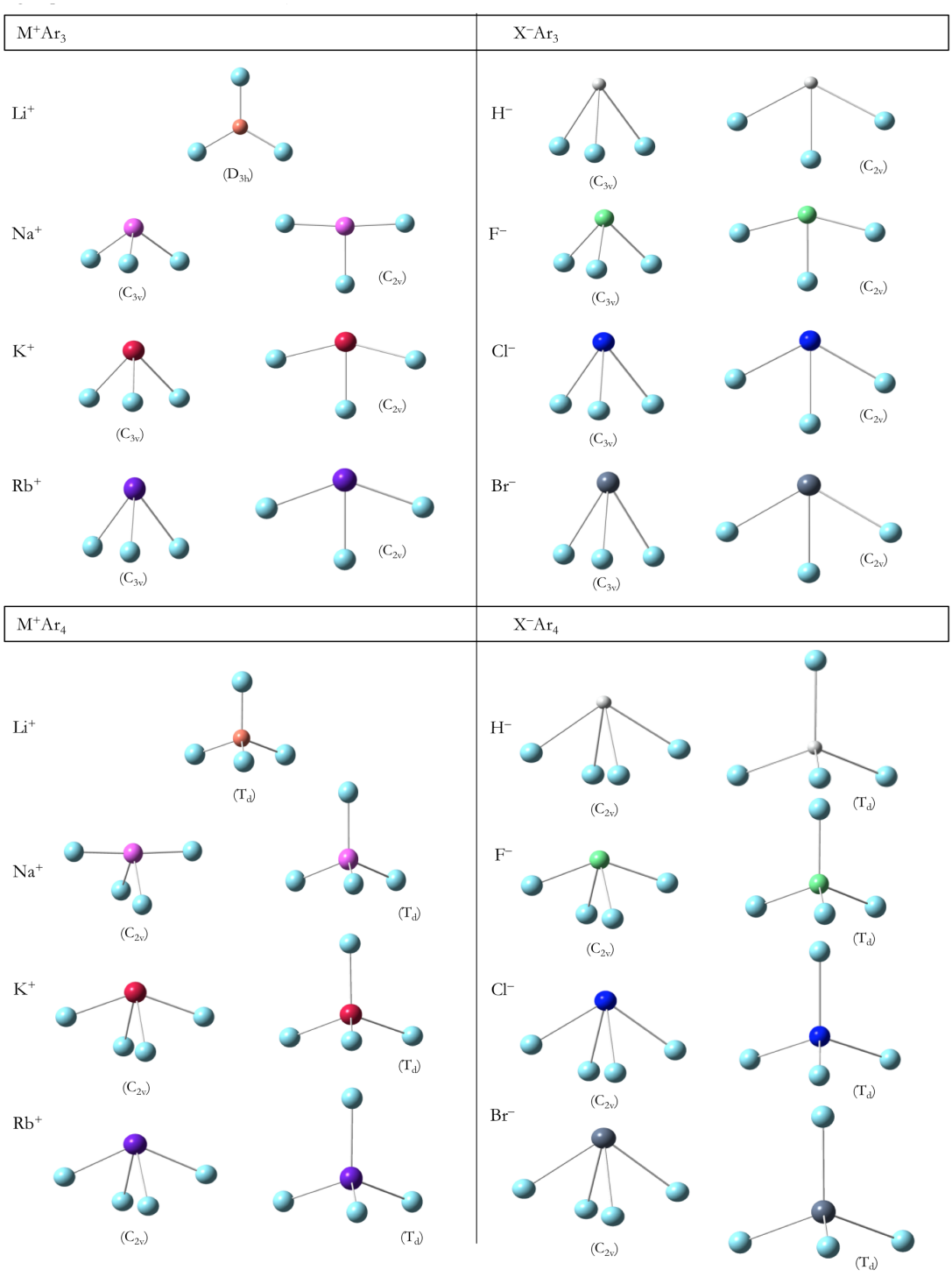

Figure 2: M^+Ar_n and X^-Ar_n clusters and their respective configurations labeled with the appropriate central ion and point group at the MP2/QZ level of theory.

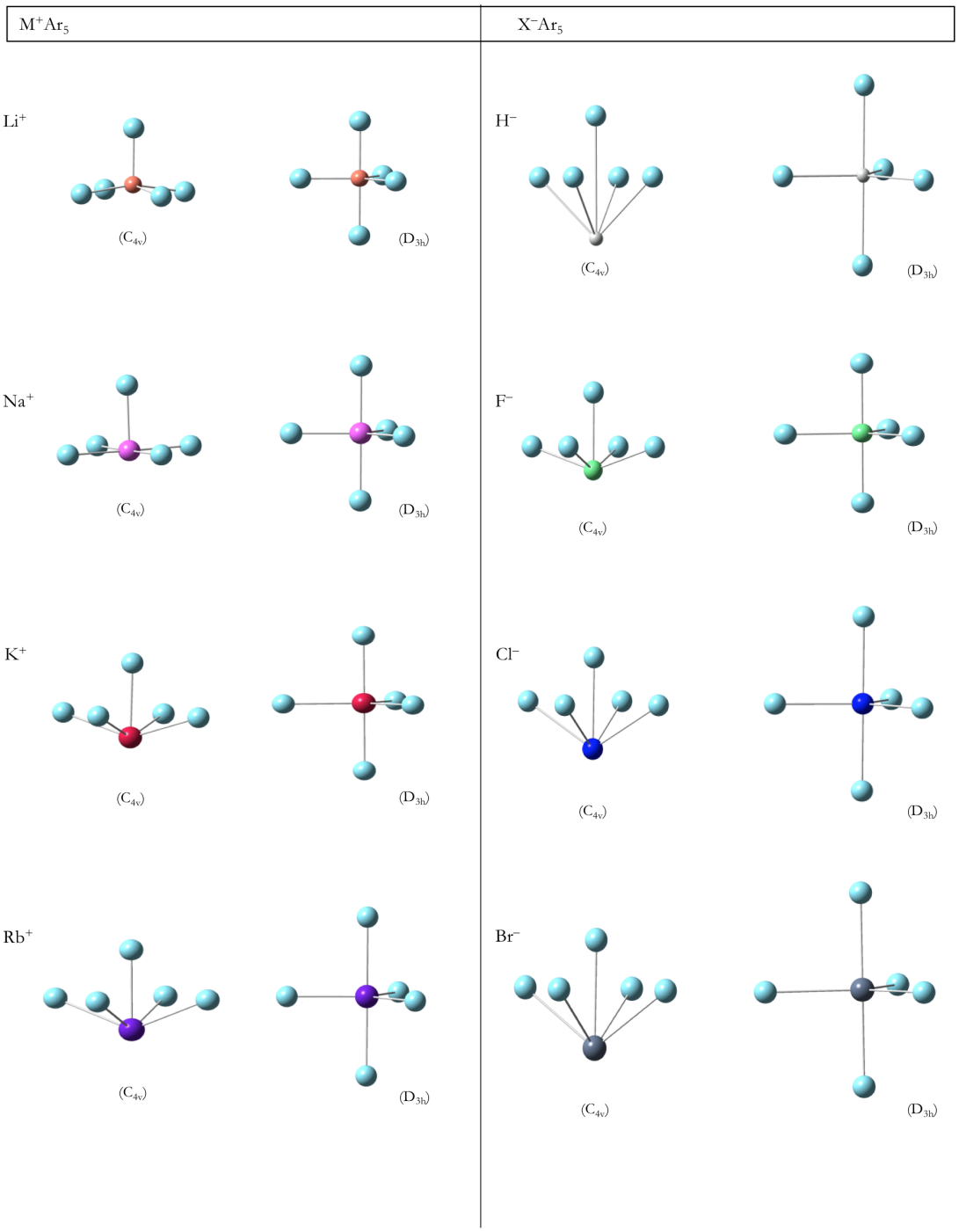

Figure 3: M^+Ar_n and X^-Ar_n clusters and their respective configurations labeled with the appropriate central ion and point group at the MP2/QZ level of theory.

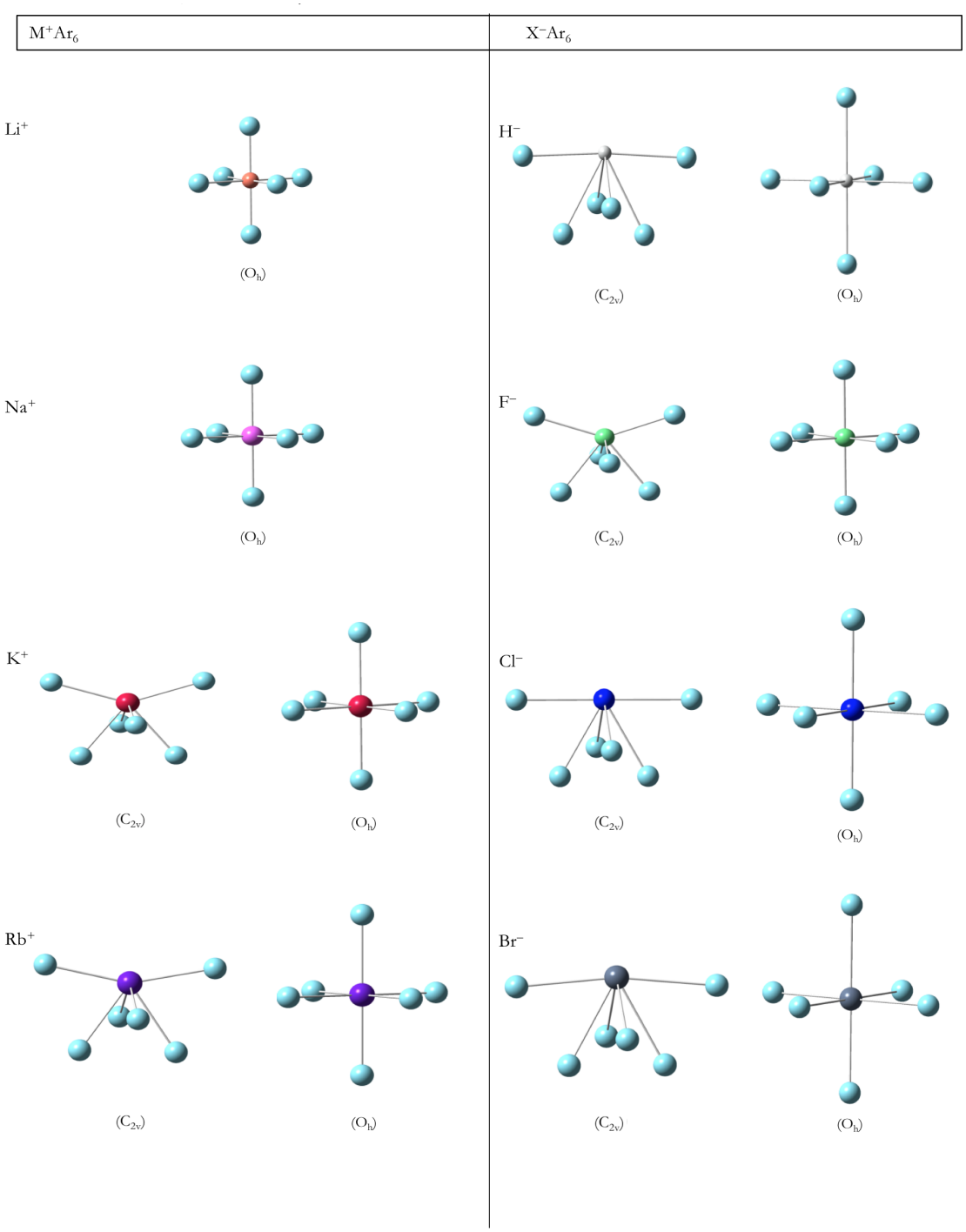

Figure 4: M^+Ar_n and X^-Ar_n clusters and their respective configurations labeled with the appropriate central ion and point group at the MP2/QZ level of theory.

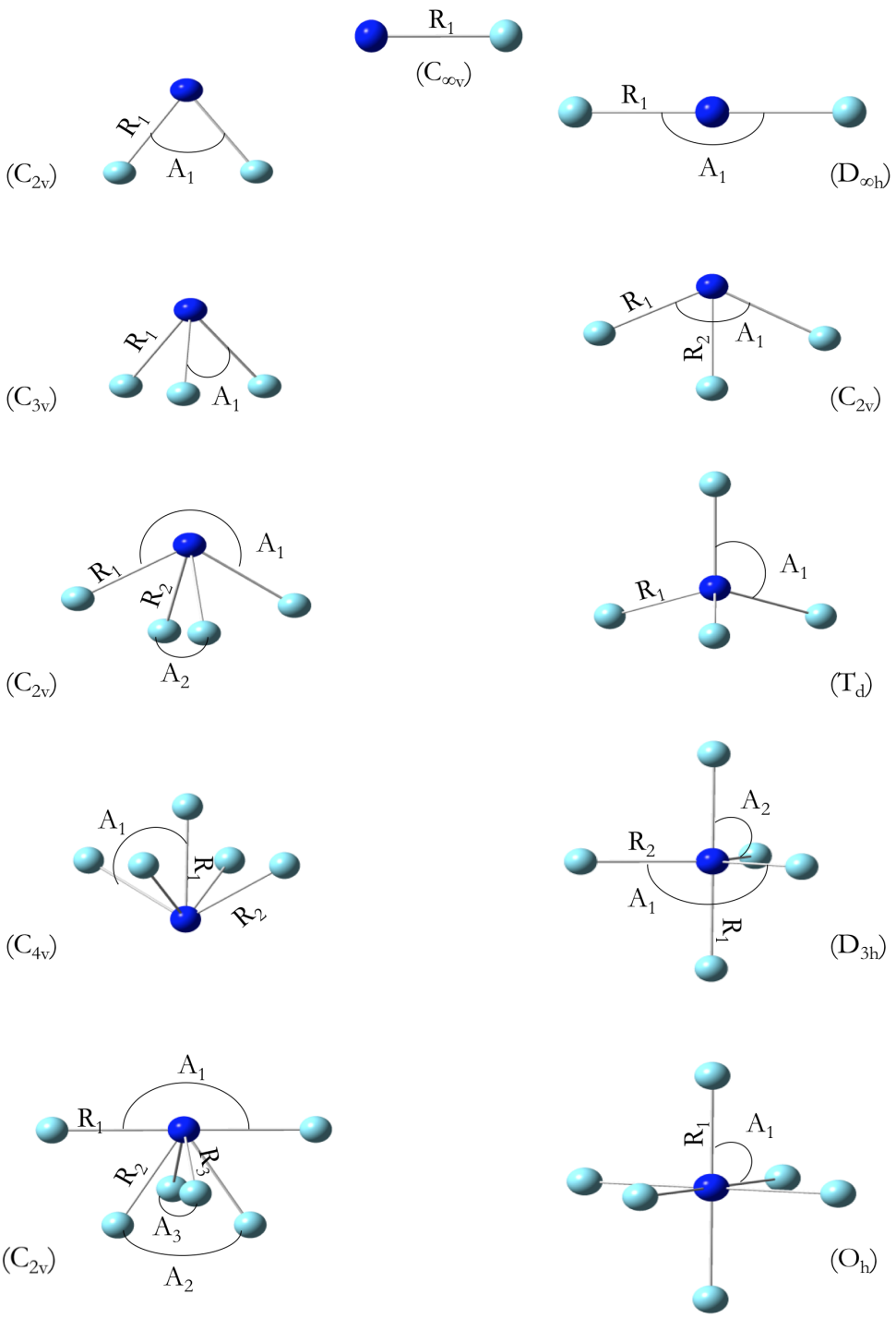

Figure 5: Unique geometrical paramters defined (interatomic distances (R) in Å and angles (A) in degrees) in relation to the corresponding point groups of each $M^{+}Ar_n$ and $X^{-}Ar_n$ configuration.

Tables 1−4 report the geometrical paramters defined in Figure 5, including various intermolecular distances (R in Å), angles (A in degrees), and point groups for the M^+Ar_n and X^-Ar_n clusters at the MP2/QZ level of theory. Figure 6 provides a visual representation of the intermolecular distances reported in Tables 1−4. Intermolecular distances are reported for each M^+Ar_n and X^-Ar_n cluster, in order of increasing ion size and number of Ar atoms. As you move down Group 1 on the periodic table (i.e., Li to Rb), intermolecular distances increase. The same trend can be seen for the anion clusters, except for H^-Ar_n where intermolecular distances are longer than those for F^-Ar_n. The longest intermolecular distance can be seen within the C_{4v} square pyramidal structure (i.e., R_1) for all M^+Ar_n and X^-Ar_n clusters except Na^+Ar_n where the longest intermolecular distance presents in the Na^+Ar_6 O_h octahedral structure.

Tables 5−8 report binding energies (only for applicable M^+Ar_n and X^-Ar_n clusters) for all configurations depicted in Figures 1−4 at the MP2/QZ and CCSD(T)/QZ levels of theory. The binding energies represent how strongly clusters are bound, whereas ΔE represents the intrinsic energetics for similar clusters. All clusters are bound, with X^-Ar_n clusters being less bound than M^+Ar_n clusters. This can be seen with the strongest bound clusters, Li^+Ar_n, and the weakest bound clusters, H^-Ar_n. For example, at the CCSD(T)/QZ level of theory, the binding energy of $Li^+Ar_4(T_d)$ is -28.05 kcal mol^{-1}, whereas the binding energy of $H^-Ar_4(T_d)$ is -3.07 kcal mol^{-1}. The deviations in binding energy among isoelectronic clusters decrease as you move down the periodic table. For example, the binding energy of $Rb^+Ar_4(T_d)$ is -12.01 kcal mol^{-1}, whereas the binding energy of $Br^-Ar_4(T_d)$ is -4.84 kcal mol^{-1}. Generally, ΔE increases between configurations as you move down the periodic table. The exception to this pattern is seen with H^-Ar_n clusters. Additionally, when comparing isoelectronic pairs, M^+Ar_n clusters have smaller relative energies than X^-Ar_n clusters.

Figure 7 depicts the sequential binding energies for all M^+Ar_n and X^-Ar_n clusters at the CCSD(T)/QZ level of theory. The sequential binding energies represent the change in binding energy as the number of Ar atoms is increased from 1 to 6 for the M^+Ar_n and X^-Ar_n clusters. Similar to the previous trends in geometrical parameters and binding energies, the deviations in sequential binding energy are largest between

Li^+Ar_n and H^-Ar_n clusters and decrease as you move down the periodic table, with the smallest deviations appearing between Rb^+Ar_n and Br^-Ar_n clusters.

Table 1: Geometrical parameters including various intermolecular distances (R in Å), angles (A in degrees), and point groups for the M^+Ar_n and X^-Ar_n clusters at the MP2/QZ level of theory.

Cluster	n	Symmetry	R_1	R_2	R_3	A_1	A_2	A_3
Li^+	1	$C_{\infty v}$	2.363	–	–	–	–	–
	2	$D_{\infty h}$	2.373	–	–	180.0	–	–
	3	D_{3h}	2.382	–	–	120.0	–	–
	4	T_d	2.402	–	–	109.5	–	–
	5	C_{4v}	2.448	2.514	–	98.1	–	–
		D_{3h}	2.552	2.466	–	120.0	90.0	–
	6	O_h	2.546	–	–	90.0	–	–
H^-	1	$C_{\infty v}$	3.714	–	–	–	–	–
	2	C_{2v}	3.727	–	–	60.0	–	–
		$D_{\infty h}$	3.713	–	–	180.0	–	–
	3	C_{3v}	3.736	–	–	59.7	–	–
		C_{2v}	3.728	3.742	–	119.5	–	–
	4	C_{2v}	3.736	3.747	–	108.6	59.5	–
		T_d	3.717	–	–	109.5	–	–
	5	C_{4v}	5.199	3.705	–	45.4	–	–
		D_{3h}	3.679	3.694	–	120.0	90.0	–
	6	C_{2v}	3.708	3.700	3.807	175.3	108.6	57.8
		O_h	3.665	–	–	90.0	–	–

Table 2: Geometrical parameters including various intermolecular distances (R in Å), angles (A in degrees), and point groups for the M^+Ar_n and X^-Ar_n clusters at the MP2/QZ level of theory.

Cluster	n	Symmetry	R_1	R_2	R_3	A_1	A_2	A_3
Na^+	1	$C_{\infty v}$	2.778	–	–	–	–	–
	2	C_{2v}	2.787	–	–	93.9	–	–
		$D_{\infty h}$	2.784	–	–	180.0	–	–
	3	C_{3v}	2.797	–	–	91.8	–	–
		C_{2v}	2.793	2.797	–	174.5	–	–
	4	C_{2v}	2.801	2.806	–	176.5	90.0	–
		T_d	2.791	–	–	109.5	–	–
	5	C_{4v}	2.814	2.811	–	89.8	–	–
		D_{3h}	2.804	2.813	–	120.0	90.0	–
	6	O_h	3.050	–	–	90.0	–	–
F^-	1	$C_{\infty v}$	3.059	–	–	–	–	–
	2	C_{2v}	3.073	–	–	74.8	–	–
		$D_{\infty h}$	3.065	–	–	180.0	–	–
	3	C_{3v}	3.086	–	–	74.2	–	–
		C_{2v}	3.078	3.088	–	148.8	–	–
	4	C_{2v}	3.090	3.101	–	139.4	73.7	–
		T_d	3.068	–	–	109.5	–	–
	5	C_{4v}	3.166	3.073	–	71.9	–	–
		D_{3h}	3.056	3.059	–	120.0	90.0	–
	6	C_{2v}	3.078	3.077	3.125	142.0	140.9	72.0
		O_h	3.050	–	–	90.0	–	–

Table 3: Geometrical parameters including various intermolecular distances (R in Å), angles (A in degrees), and point groups for the M^+Ar_n and X^-Ar_n clusters at the MP2/QZ level of theory.

Cluster	n	Symmetry	R_1	R_2	R_3	A_1	A_2	A_3
K^+	1	$C_{\infty v}$	3.188	–	–	–	–	–
	2	C_{2v}	3.195	–	–	75.0	–	–
		$D_{\infty h}$	3.197	–	–	180.0	–	–
	3	C_{3v}	3.199	–	–	74.5	–	–
		C_{2v}	3.201	3.200	–	149.9	–	–
	4	C_{2v}	3.206	3.205	–	139.7	74.1	–
		T_d	3.197	–	–	109.5	–	–
	5	C_{4v}	3.237	3.195	–	72.2	–	–
		D_{3h}	3.187	3.191	–	120.0	90.0	–
	6	C_{2v}	3.204	3.196	3.221	142.5	–	–
		O_h	3.182	–	–	90.0	–	–
Cl^-	1	$C_{\infty v}$	3.666	–	–	–	–	–
	2	C_{2v}	3.673	–	–	61.1	–	–
		$D_{\infty h}$	3.668	–	–	180.0	–	–
	3	C_{3v}	3.678	–	–	60.9	–	–
		C_{2v}	3.674	3.681	–	121.8	–	–
	4	C_{2v}	3.679	3.685	–	110.9	60.7	–
		T_d	3.664	–	–	109.5	–	–
	5	C_{4v}	3.799	3.649	–	58.6	–	–
		D_{3h}	3.653	3.656	–	120.0	90.0	–
	6	C_{2v}	3.668	3.665	3.708	179.9	111.1	59.6
		O_h	3.646	–	–	90.0	–	–

Table 4: Geometrical parameters including various intermolecular distances (R in Å), angles (A in degrees), and point groups for the M^+Ar_n and X^-Ar_n clusters at the MP2/QZ level of theory.

Cluster	n	Symmetry	R_1	R_2	R_3	A_1	A_2	A_3
Rb^+	1	$C_{\infty v}$	3.361	–	–	–	–	–
	2	C_{2v}	3.366	–	–	70.0	–	–
		$D_{\infty h}$	3.373	–	–	180.0	–	–
	3	C_{3v}	3.370	–	–	69.5	–	–
		C_{2v}	3.374	3.372	–	139.1	–	–
	4	C_{2v}	3.378	3.376	–	128.5	69.2	–
		T_d	3.370	–	–	109.5	–	–
	5	C_{4v}	3.422	3.365	–	67.0	–	–
		D_{3h}	3.364	3.364	–	120.0	90.0	–
	6	C_{2v}	3.380	3.369	3.395	156.7	129.1	67.2
		O_h	3.359	–	–	90.0	–	–
Br^-	1	$C_{\infty v}$	3.871	–	–	–	–	–
	2	C_{2v}	3.876	–	–	57.6	–	–
		$D_{\infty h}$	3.872	–	–	180.0	–	–
	3	C_{3v}	3.880	–	–	57.4	–	–
		C_{2v}	3.875	3.883	–	114.9	–	–
	4	C_{2v}	3.879	3.886	–	104.0	57.3	–
		T_d	3.867	–	–	109.5	–	–
	5	C_{4v}	4.023	3.847	–	55.2	–	–
		D_{3h}	3.857	3.859	–	120.0	90.0	–
	6	C_{2v}	3.868	3.865	3.908	169.9	104.1	56.3
		O_h	3.851	–	–	90.0	–	–

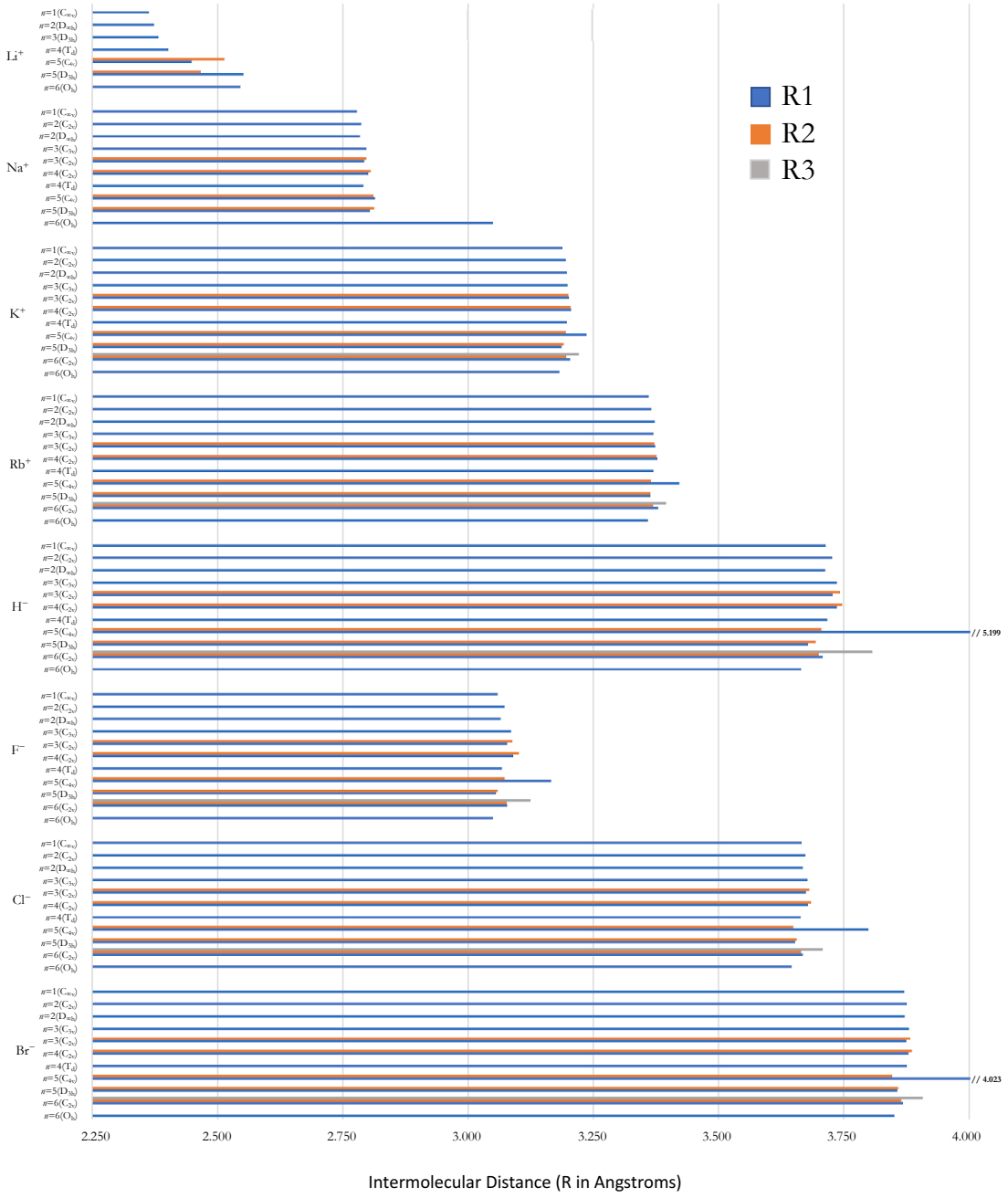

Figure 6: Intermolecular distances (R in Å) for the M^+Ar_n and X^-Ar_n clusters at the MP2/QZ level of theory.

Table 5: Electronic binding energies (E_{bind} in kcal mol^{-1}) and relative electronic energies(ΔE in kcal mol^{-1}) for the M^+Ar_n and X^-Ar_n clusters at both the MP2/QZ and CCSD(T)/QZ level of theory.

			E_{bind}		ΔE	
Cluster	n	Symmetry	MP2	CCSD(T)	MP2	CCSD(T)
Li^+	1	$C_{\infty v}$	−6.87	−6.91	–	–
	2	$D_{\infty h}$	−13.33	−13.39	–	–
	3	D_{3h}	−19.40	−19.41	–	–
	4	T_d	−25.10	−24.95	–	–
	5	C_{4v}	−28.60	−28.10	0.00	0.00
		D_{3h}	−28.53	−28.05	+0.07	+0.05
	6	O_h	−32.97	−32.09	–	–
H^-	1	$C_{\infty v}$	−0.84	−0.75	–	–
	2	C_{2v}	−1.96	−1.71	0.00	0.00
		$D_{\infty h}$	−1.69	−1.50	+0.27	+0.20
	3	C_{3v}	−3.36	−2.89	0.00	0.00
		C_{2v}	−3.08	−2.68	+0.28	+0.21
	4	C_{2v}	−4.78	−4.09	0.00	0.00
		T_d	−3.43	−3.07	+1.35	+1.03
	5	C_{4v}	−6.16	−5.24	0.00	0.00
		D_{3h}	−4.44	−3.95	+1.72	+1.30
	6	C_{2v}	−7.19	−6.17	0.00	0.00
		O_h	−5.48	−4.86	+1.71	+1.31

Table 6: Electronic binding energies (E_{bind} in kcal mol^{-1}) and relative electronic energies(ΔE in kcal mol^{-1}) for the M^+Ar_n and X^-Ar_n clusters at both the MP2/QZ and CCSD(T)/QZ level of theory.

			E_{bind}		ΔE	
Cluster	n	Symmetry	MP2	CCSD(T)	MP2	CCSD(T)
Na^+	1	$C_{\infty v}$	−3.92	−3.94	–	–
	2	C_{2v}	−7.75	−7.76	0.00	+0.01
		$D_{\infty h}$	−7.73	−7.77	+0.02	0.00
	3	C_{3v}	−11.56	−11.51	0.00	0.00
		C_{2v}	−11.50	−11.49	+0.06	+0.02
	4	C_{2v}	−15.31	−15.19	0.00	0.00
		T_d	−15.11	−15.09	+0.20	+0.10
	5	C_{4v}	−19.09	−18.83	0.00	0.00
		D_{3h}	−18.92	−18.73	+0.16	+0.10
	6	O_h	−22.94	−22.51	–	–
F^-	1	$C_{\infty v}$	−2.25	−2.48	–	–
	2	C_{2v}	−4.65	−4.90	0.00	0.00
		$D_{\infty h}$	−4.47	−4.90	+0.19	+0.11
	3	C_{3v}	−7.24	−7.61	0.00	0.00
		C_{2v}	−7.02	−7.49	+0.21	+0.13
	4	C_{2v}	−9.80	−10.19	0.00	0.00
		T_d	−8.90	−9.66	+0.90	+0.54
	5	C_{4v}	−12.26	−12.70	0.00	0.00
		D_{3h}	−11.48	−12.29	+0.77	+0.42
	6	C_{2v}	−14.70	−15.19	0.00	0.00
		O_h	−14.17	−14.97	+0.53	+0.22

Table 7: Electronic binding energies (E_{bind} in kcal mol^{-1}) and relative electronic energies(ΔE in kcal mol^{-1}) for the M^+Ar_n and X^-Ar_n clusters at both the MP2/QZ and CCSD(T)/QZ level of theory.

			E_{bind}		ΔE	
Cluster	n	Symmetry	MP2	CCSD(T)	MP2	CCSD(T)
K^+	1	$C_{\infty v}$	−2.65	−2.54	–	–
	2	C_{2v}	−5.42	−5.14	0.00	0.00
		$D_{\infty h}$	−5.26	−5.03	+0.16	+0.11
	3	C_{3v}	−8.34	−7.85	0.00	0.00
		C_{2v}	−8.12	−7.70	+0.22	+0.16
	4	C_{2v}	−11.23	−10.52	0.00	0.00
		T_d	−10.43	−9.93	+0.80	+0.59
	5	C_{4v}	−14.05	−13.12	0.00	0.00
		D_{3h}	−13.37	−12.65	+0.69	+0.48
	6	C_{2v}	−16.84	−15.70	0.00	0.00
		O_h	−16.37	−12.65	+0.47	+0.31
Cl^-	1	$C_{\infty v}$	−1.47	−1.41	–	–
	2	C_{2v}	−3.19	−3.01	0.00	0.00
		$D_{\infty h}$	−2.93	−2.83	+0.26	+0.18
	3	C_{3v}	−5.18	−4.80	0.00	0.00
		C_{2v}	−4.90	−4.60	+0.28	+0.20
	4	C_{2v}	−7.17	−6.58	0.00	0.00
		T_d	−5.87	−5.63	+1.30	+0.95
	5	C_{4v}	−8.83	−8.09	0.00	0.00
		D_{3h}	−7.49	−7.13	+1.33	+0.96
	6	C_{2v}	−10.74	−9.83	0.00	0.00
		O_h	−9.16	−8.67	+1.58	+1.16

Table 8: Electronic binding energies (E_{bind} in kcal mol^{-1}) and relative electronic energies(ΔE in kcal mol^{-1}) for the M^+Ar_n and X^-Ar_n clusters at both the MP2/QZ and CCSD(T)/QZ level of theory.

			E_{bind}		ΔE	
Cluster	n	Symmetry	MP2	CCSD(T)	MP2	CCSD(T)
Rb^+	1	$C_{\infty v}$	−2.39	−2.27	–	–
	2	C_{2v}	−4.94	−4.64	0.00	0.00
		$D_{\infty h}$	−4.72	−4.47	+0.23	+0.17
	3	C_{3v}	−7.72	−7.17	0.00	0.00
		C_{2v}	−7.44	−6.96	+0.28	+0.21
	4	C_{2v}	−10.45	−9.66	0.00	0.00
		T_d	−9.41	−8.88	+1.04	+0.78
	5	C_{4v}	−13.01	−12.01	0.00	0.00
		D_{3h}	−12.02	−11.28	+0.99	+0.74
	6	C_{2v}	−15.59	−14.38	0.00	0.00
		O_h	−14.64	−13.66	+0.95	+0.72
Br^-	1	$C_{\infty v}$	−1.28	−1.21	–	–
	2	C_{2v}	−2.83	−2.62	0.00	0.00
		$D_{\infty h}$	−2.56	−2.42	+0.27	+0.20
	3	C_{3v}	−4.67	−4.24	0.00	0.00
		C_{2v}	−4.39	−4.03	+0.29	+0.21
	4	C_{2v}	−6.52	−5.86	0.00	0.00
		T_d	−5.15	−4.84	+1.37	+1.02
	5	C_{4v}	−7.89	−7.17	0.00	0.00
		D_{3h}	−6.55	−6.12	+1.43	+1.05
	6	C_{2v}	−9.76	−8.75	0.00	0.00
		O_h	−7.99	−7.42	+1.77	+1.33

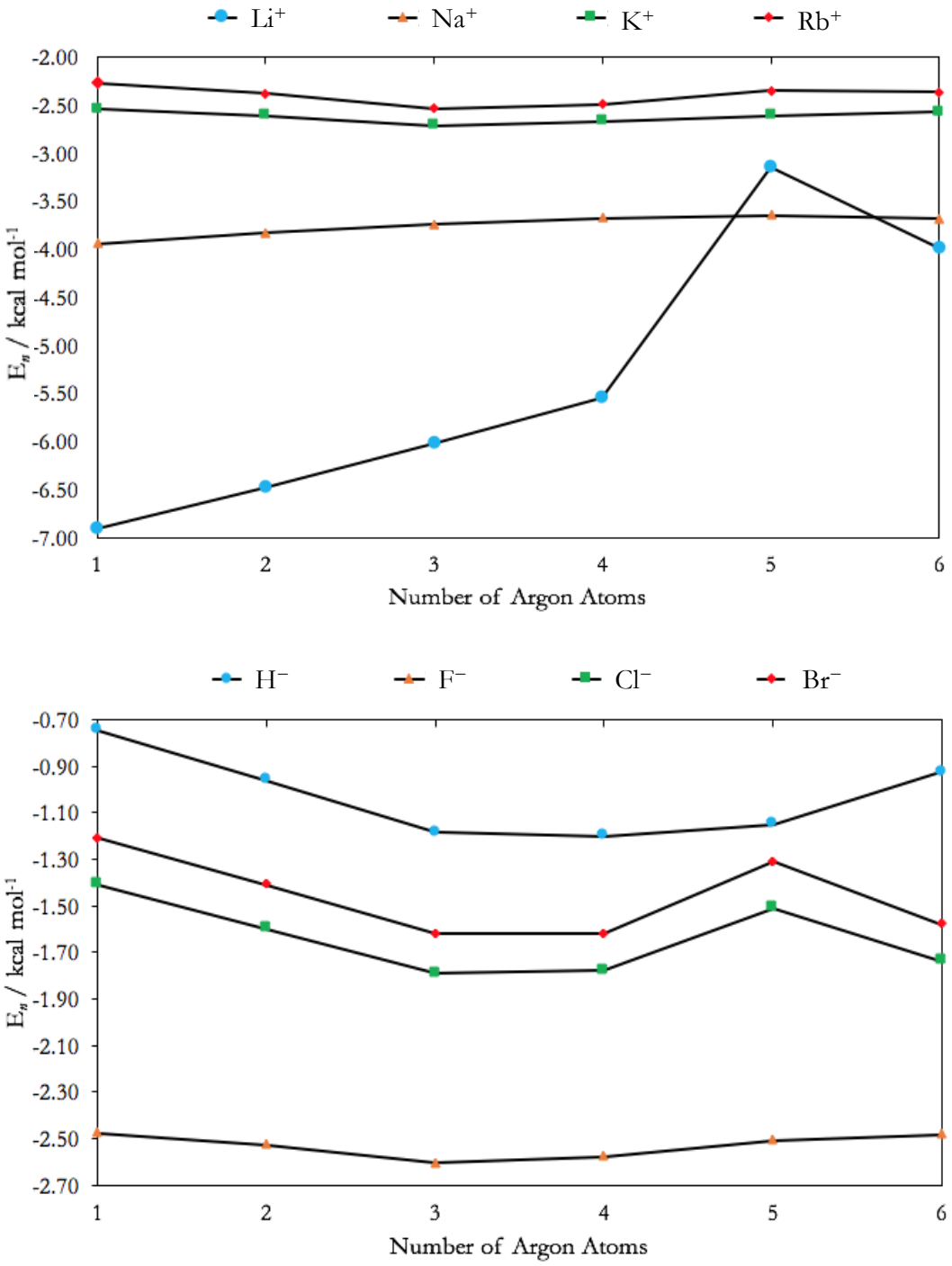

Figure 7: Sequential binding energies (E_n in kcal mol^{-}) for the $M^{+}Ar_n$ and $X^{-}Ar_n$ (where n=1−6) clusters at the CCSD(T)/QZ level of theory.

4 Conclusions

This study provides a thorough characterization of the M^+Ar_n and X^-Ar_n systems via full geometry optimizations and vibrational frequency computations with sophisticated *ab initio* levels of theory. As an extension of the previous literature[22–26] we identified low-energy configurations for Li^+Ar_n and Na^+Ar_n systems where n=1−6, as well as for the analogous K^+Ar_n and Rb^+Ar_n systems. Additionally, we were able to fully characterize the corresponding isoelectronic anion clusters (i.e., H^-Ar_n, F^-Ar_n, Cl^-Ar_n, and Br^-Ar_n, respectively). Generally, the low-energy minima for each system agree with those reported in the previous literature. Consistent with patterns seen among the Li^+Ar_n and Na^+Ar_n investigations, two low-energy minima were identified for most clusters where $n\geq2$, whereas only one minimum was identified for Na^+Ar_6 and for Li^+Ar_n where n=2, 3, 4 and 6.

A general trend is seen among solvated structures for all M^+Ar_n and X^-Ar_n clusters, where the lowest energy configurations were in agreement across most systems. Deviations in lowest-energy configurations are seen among Li^+Ar_n where n=2, 3, 4 and 6 and Na^+Ar_6 in comparison to the other M^+Ar_n and X^-Ar_n configurations. Additional low energy configurations for larger clusters (i.e., M^+Ar_n and X^-Ar_n where n=5 and 6) not seen in previous literature or found within the Li^+Ar_n and Na^-Ar_n were identified and reported within this investigation. The lowest energy configurations are typically those that show favorable Ar-Ar attractions (i.e., atypical configurations).

In general, M^+Ar_n clusters are more strongly bound than X^-Ar_n clusters, with deviations in E_{bind} among isoelectronic clusters decreasing with progression down the periodic table (i.e., Li to Rb and H to Br). Additionally, M^+Ar_n clusters have smaller relative energies than X^-Ar_n clusters. ΔE generally increases between low-energy configurations decreasing with progression down the periodic table, with the exception appearing for H^-Ar_n clusters.

The thorough characterization of the M^+Ar_n and X^-Ar_n isoelectronic systems

found within this investigation will provide valuable information on similar systems in future experimental and theoretical investigations of explicit microsolvation of ions by noble gas atoms.

References

[1] D. Prekas, C. Luder, and M. Velegrakis, *J. Phys. Chem.*, **108**, 4450 (1998). Structural transitions in metal ion-doped noble gas clusters: Experiments and molecular dynamics simulations. http://dx.doi.org/10.1063/1.475856.

[2] M. Slama, K. Issa, F. B. Mohamed, M. B. E. H. Rhouma, and F. Spiegelman, *Eur. Phys. J. D*, **70**, 242 (2016). Structure and stability of Na^+Xe_n clusters. http://dx.doi.org/10.1140/epjd/e2016-70147-0.

[3] C. D. Paola, F. Sebastianelli, E. Bodo, I. Baccarelli, and F. A. Gianturco, *J. Chem. Theory Comput.*, **70**, 1045 (2005). Microsolvation of Li^+ in Small He Clusters. Li^+He_n Species from Classical and Quantum Calculations. http://dx.doi.org/10.1021/ct050072m.

[4] W. Breckenridge, V. L. Ayles, and T. G. Wright, *Chemical Physics*, **333**, 77 (2007). Analysis of the bonding in alkali-cation/Rg complexes (Rg = He-Xe) using a simple model potential. http://dx.doi.org/10.1016/j.chemphys.2007.01.008.

[5] A. M. Gardner, C. D. Withers, J. B. Graneek, T. G. Wright, L. A. Viehland, and W. H. Breckenridge, *J. Phys. Chem. A*, **114**, 7631 (2010). Theoretial Study of M^+-RG and M^{2+}-RG Complexes and Transport of M^+ through RG (M = Be and MG, RG = He-Rn). http://dx.doi.org/10.1021/jp103836t.

[6] P. Soldan, E. P. Lee, J. Lozeille, J. N. Murrell, and T. G. Wright, *Chemical Physics Letters*, **343**, 429 (2001). High-quality interatomic potential for Li^+·He. http://dx.doi.org/10.1016/S0009-2614(01)00717-5.

[7] M. F. McGuirk, L. A. Viehland, E. P. F. Lee, W. H. Breckenridge, C. D. Withers, A. M. Garder, R. J. Plowright, and T. G. Wright, *J. Chem. Phys*, **130**, 194305 (2009). Theoretical study of Ba^{n+}-RG (RG=rare gas) complexes and transport of Ba^{n+} through RG (n - 1,2; RG=He-Rn). http://dx.doi.org/10.1063/1.3132543.

[8] A. M. Gardner, C. D. Withers, T. G. Wright, K. I. Kaplan, C. Y. N. Chapman, L. A. Viehland, E. P. F. Lee, and W. H. Breckenridge, *J. Chem. Phys*, **132**, 054302 (2010). Theoretical study of bonding in M^{n+}-RG complexes and the transport of M^{n+} through rare gas (M = Ca, Sr, and Ra; n = 1 and 2; and RG=He-Rn). http://dx.doi.org/10.1063/1.3297891.

[9] S. H. Pullins, C. T. Scurlock, J. E. Reddic, and M. A. Duncan, *J. Chem. Phys.*, **104**, 7518 (1996). Photodissociation spectroscopy of Ca^+-rare gas complexes. http://dx.doi.org/10.1063/1.471653.

[10] J. S. Pilgrim, C. S. Yeh, K. R. Berry, and M. A. Duncan, *J. Chem. Phys.*, **100**, 7945 (1994). Photodissociation spectroscopy of Mg^+-rare gas complexes. http://dx.doi.org/10.1063/1.466840.

[11] C. T. Scurlock, J. S. Pilgrim, and M. A. Duncan, *J. Chem. Phys.*, **103**, 3293 (1995). Rotationally resolved photodissociation spectroscopy of Mg^+-Ar. http://dx.doi.org/10.1063/1.470683.

[12] J. Lozeille, E. Winata, P. Soldan, E. P. F. Lee, L. A. Viehland, and T. G. Wright, *Phys. Chem. Chem. Phys.*, **4**, 3601 (2002). Spectroscopy of Li^+·Rg and Li^+-Rg transport coefficients (Rg = He-Rn). http://dx.doi.org/10.1039/b111675d.

[13] L. A. Viehland, J. Lozeille, P. Soldan, E. P. F. Lee, and T. G. Wright, *J. Chem. Phys.*, **119**, 3729 (2003). Spectroscopy of Na^+·Rg and transport coefficients o Na^+ in Rg(Rg=He-Rn). http://dx.doi.org/10.1063/1.1591171.

[14] R. Ahlrichs, H. J. Bohm, S. Brode, K. T. Tang, and J. P. Toennies, *J. Chem. Phys.*, **88**, 6290 (1988). Interaction potentials for alkali ion-rare gas and halogen ion-rare gas systems. http://dx.doi.org/10.1063/1.454467.

[15] N. Issaoui, K. Abdessalem, H. Ghalla, S. J. Yaghmour, F. Calvo, and B. Oujia, *J. Chem. Phys.*, **141**, 174316 (2014). Theoretical investigation of the relative stablility of Na^+He_n (n = 2-24) clusters: Many-body versus delocalization effects. http://dx.doi.org/10.1063/1.4900873.

[16] K. Abdessalem, H. Habli, H. Ghalla, S. J. Yaghmour, F. Calvo, and B. Oujia, *J. Chem. Phys.*, **141**, 154308 (2014). Many-body effects on the structures and stability of $Ba^{2+}Xe_n$ (n = 1-39, 54) clusters. http://dx.doi.org/10.1063/1.4896607.

[17] G. S. Fanourgakis, S. C. Farantos, C. Luder, and M. Velegrakis, *J. Chem. Phys.*, **109**, 108 (1998). Photofragmentation spectra and structures of Sr^+Ar_n, n=2-8 clusters: Experiment and theory. http://dx.doi.org/10.1063/1.476527.

[18] L. A. Viehland, J. Lozeille, P. Soldan, E. P. F. Lee, and T. G. Wright, *J. Chem. Phys.*, **121**, 341 (2004). Spectroscopy of K^+·Rg and transport coefficients of K^+ in Rg (Rg=He-Rn). http://dx.doi.org/10.1063/1.1735560.

[19] H. L. Hickling, L. A. Viehland, D. T. Shepherd, P. Soldan, E. P. F. Lee, and T. G. Wright, *Phys. Chem. Chem. Phys.*, **6**, 4233 (2004). Spectroscopy of M^+·Rg and transport coefficients of M^+ in Rg (M = Rb-Fr; Rg = He-Rn). http://dx.doi.org/10.1039/b405221h.

[20] M. Slama, K. Issa, M. Zbidi, and M. B. E. H. Rhouma, *Molecular Physics*, **115:6**, 757 (2017). Microsolvation of K^+ in xenon clusters: a three-body approximation and structural transition. http://dx.doi.org/10.1080/00268976.2017.1284353.

[21] F. Grandinetti, *Eur. J. Mass Spectrom.*, **17**, 423 (2011). Gas-phase ion chemistry of the noble gases: recent advances and future perspectives. http://dx.doi.org/10.1255/ejms.1151.

[22] J. J. Szymczak, K. T. Giju, S. Roszak, and J. Leszczynski, *J. Phys. Chem. A*, **108**, 6570 (2004). The Li^+ Cation-The Descendant of H^+ or an Ancestor of Na^+? The Properties of Li^+Ar_n (n = 1-6) Clusters. http://dx.doi.org/10.1021/jp049103k.

[23] F. V. Prudente, J. M. C. Marques, and F. B. Pereira, *Phys.Chem.Chem.Phys.*, **19**, 25707 (2017). Solvation of Li^+ by argon: how important are three-body forces? http://dx.doi.org/10.1039/c7cp04549b.

[24] T. Nagata, M. Aoyagi, and S. Iwata, *J. Phys. Chem. A*, **108**, 683 (2004). Noble Gas Clusters Doped with a Metal Ion I: Ab Initio Studies of Na^+Ar_n. http://dx.doi.org/10.1021/jp036443h.

[25] K. T. Giju, S. Roszak, R. W. Gora, and J. Leszczynski, *Chemical Physics Letters*, **391**, 112 (2004). The micro-solvation of Na^+: theoretical study of bonding characteristics in weakly bonded Ar_nNa^+ (n = 1-8) clusters. http://dx.doi.org/10.1016/j.cplett.2004.04.085.

[26] M. B. E. H. Rhouma, F. Calvo, and F. Spiegelman, *J. Phys. Chem. A*, **110**, 5010 (2006). Solvation of Na^+ in Argon Clusters. http://dx.doi.org/10.1021/jp060153u.

[27] V. Vallet, G. Bendazzoli, and S. Evangelisti, *Chemical Physics*, **263**, 33 (2001). Ab initio study of the ground-state potential of XH^- anions (X = He, Ne, Ar). http://dx.doi.org/10.1016/S0301-0104(00)00356-6.

[28] B. R. Gray, T. G. Wright, E. L. Wood, and L. A. Viehland, *Phys. Chem. Chem. Phys.*, **8**, 4752 (2006). Accurate potential energy curves for F^--Rg (Rg = He-Rn): Spectroscopy and transport coefficients. http://dx.doi.org/10.1039/b610476b.

[29] C. D. Withers, T. G. Wright, L. A. Viehland, L. Grossman, C. C. Kirkpatrick, and E. P. F. Lee, *J. Chem. Phys.*, **135**, 024312 (2011). Theoretical study of Cl^-RG (rare gas) complexes and transport of Cl^- through RG (RG = He-Rn). http://dx.doi.org/10.1063/1.3598472.

[30] A. Wada, A. Kikkawa, T. Sugiyama, and K. Hiraoka, *International Journal of mass Spectrometry*, **267**, 284 (2007). Thermochemical stabilities of the gas-phase cluster ions of halide ions with rare gas atoms. http://dx.doi.org/10.1016/j.ijms.2007.02.053.

[31] F. Sebastianelli, I. Baccarelli, C. D. Paola, and F. A. Gianturco, *J. Chem. Phys.*, **119**, 5570 (2003). Structural and quantum effects from an-

ionic centers in rare gas clusters: The $(Ne)_nH^-$ and $(Ne)_{n+1}$ systems. http://dx.doi.org/10.1063/1.1599343.

[32] I. Yourshaw, Y. Zhao, and D. M. Neumark, *J. Chem. Phys.*, **105**, 351 (1996). Many-body effects in weakly bound anion and neutral clusters: Zero electron kinetic energy spectroscopy and threshold photodetachment spectroscopy of $Ar-nBr^-$ (n=2-9) and Ar_nI^- (n=2-19). http://dx.doi.org/10.1063/1.471893.

[33] T. Lenzer, I. Yourshaw, M. R. Furlanetto, N. L. Pivonka, and D. M. Neumark, *J. Chem. Phys.*, **115**, 3578 (2001). Characterization of $Ar_nCl^(-)$ clusters (n=2-15) using zero electron kinetic energy and partially discriminated threshold photodetachment spectroscopy. http://dx.doi.org/10.1063/1.1388202.

[34] C. Møller and M. S. Plesset, *Phys. Rev.*, **46**, 618 (1934). Note on an Approximation Treatment for Many-electron Systems. http://dx.doi.org/10.1103/PhysRev.46.618.

[35] R. A. Kendall, T. H. Dunning, and R. J. Harrison, *J. Chem. Phys.*, **96**, 6796 (1992). Electron affinities of the first-row atoms revisited. Systematic basis sets and wave functions. http://dx.doi.org/10.1063/1.462569.

[36] D. E. Woon and T. H. Dunning, *J. Chem. Phys.*, **98**, 1358 (1993). Gaussian Basis Sets for Use in Correlated Molecular Calculations. III. The second row atoms, Al-Ar. http://dx.doi.org/10.1063/1.464303.

[37] A. K. Wilson, D. E. Woon, K. A. Peterson, and T. H. Dunning, *J. Chem. Phys.*, **110**, 7667 (1999). Gaussian basis sets for use in correlated molecular calculations. IX. The atoms gallium through krypton. http://dx.doi.org/10.1063/1.478678.

[38] B. P. Prascher, D. E. Woon, K. A. Peterson, T. H. Dunning, and A. K. Wilson, *Theor. Chem. Acc.*, **128**, 69 (2011). Gaussian basis sets for use in correlated molecular calculations. VII. Valence and core-valence basis sets for Li,Na,Be, and Mg. http://dx.doi.org/10.1007/s00214-010-0764-0.

[39] J. G. Hill and K. A. Peterson, *J. Chem. Phys.*, **147**, 244106 (2017). Gaussian basis sets for use in correlated molecular calculations. XI. Pseudopotential-based and all-electron relativistic basis sets for alkali metal (K-Fr) and alkaline earth (Ca-Ra) elements. http://dx.doi.org/10.1063/1.5010587.

[40] R. J. Bartlett, *WIREs Comput. Mol Sci.*, **2**, 126 (2012). Coupled-cluster Theory and its Equation-of-motion Extensions. http://dx.doi.org/10.1002/wcms.76.

[41] K. Raghavachari, G. W. Trucks, J. A. Pople, and M. Head-Gordon, *Chem. Phys. Let.*, **157**, 479 (1989). A Fifth-order Perturbation Comparison of Electron Correlation Theories. http://dx.doi.org/10.1016/50009-2614(89)87395-6.

[42] M. J. Frisch, G. W. Trucks, H. B. Schlegel, G. E. Scuseria, M. A. Robb, J. R. Cheeseman, G. Scalmani, V. Barone, G. A. Petersson, H. Nakatsuji, X. Li, M. Caricato, A. V. Marenich, J. Bloino, B. G. Janesko, R. Gomperts, B. Mennucci, H. P. Hratchian, J. V. Ortiz, A. F. Izmaylov, J. L. Sonnenberg, D. Williams-Young, F. Ding, F. Lipparini, F. Egidi, J. Goings, B. Peng, A. Petrone, T. Henderson, D. Ranasinghe, V. G. Zakrzewski, J. Gao, N. Rega, G. Zheng, W. Liang, M. Hada, M. Ehara, K. Toyota, R. Fukuda, J. Hasegawa, M. Ishida, T. Nakajima, Y. Honda, O. Kitao, H. Nakai, T. Vreven, K. Throssell, J. A. Montgomery, Jr., J. E. Peralta, F. Ogliaro, M. J. Bearpark, J. J. Heyd, E. N. Brothers, K. N. Kudin, V. N. Staroverov, T. A. Keith, R. Kobayashi, J. Normand, K. Raghavachari, A. P. Rendell, J. C. Burant, S. S. Iyengar, J. Tomasi, M. Cossi, J. M. Millam, M. Klene, C. Adamo, R. Cammi, J. W. Ochterski, R. L. Martin, K. Morokuma, O. Farkas, J. B. Foresman, and D. J. Fox, 2016, gaussian Inc. Wallingford CT. Gaussian16 Revision B.01.

[43] H.-J. Werner, P. J. Knowles, G. Knizia, F. R. Manby, M. Schütz, P. Celani, W. Györffy, D. Kats, T. Korona, R. Lindh, A. Mitrushenkov, G. Rauhut, K. R. Shamasundar, T. B. Adler, R. D. Amos, A. Bernhardsson, A. Berning, D. L. Cooper, M. J. O. Deegan, A. J. Dobbyn, F. Eckert, E. Goll, C. Hampel, A. Hesselmann, G. Hetzer, T. Hrenar, G. Jansen, C. Köppl, Y. Liu, A. W. Lloyd,

R. A. Mata, A. J. May, S. J. McNicholas, W. Meyer, M. E. Mura, A. Nicklass, D. P. O'Neill, P. Palmieri, D. Peng, K. Pflüger, R. Pitzer, M. Reiher, T. Shiozaki, H. Stoll, A. J. Stone, R. Tarroni, T. Thorsteinsson, and M. Wang, 2015, http://www.molpro.net. MOLPRO, version 2015.1, a package of ab initio programs.

[44] I. Lim, P. Schwerdtfeger, B. Metz, and H. Stoll, *J. Chem. Phys.*, **122**, 104103 (2005). All-electron and relativistic pseudopotential studies for the group 1 element polarizabilities from K to element 119. http://dx.doi.org/10.1063/1.1856451.

[45] H. Stoll, B. Metz, and M. Dolg, *J. Comput. Chem.*, **23**, 767 (2002). Relativistic energy-consistent pseudopotentials–recent developments. http://dx.doi.org/10.1002/jcc.10037.

[46] R. J. Gillespie, *J. Chem. Educ.*, **40(6)**, 295 (1963). The valence-shell electron-pair repulsion (VSEPR) theory of directed valency. http://dx.doi.org/10.1021/ed040p295.

Appendix

Table A1: Cartesian coordinates in Angstroms (Å) for the $C_{\infty v}$ optimized geometry of Li^+Ar at the MP2/TZ level of theory.

Atom	x	y	z
Li	0.000000	0.000000	−0.011829
Ar	0.000000	0.000000	−2.388171

Table A2: Cartesian coordinates in Angstroms (Å) for the $D_{\infty h}$ optimized geometry of Li^+Ar_2 at the MP2/TZ level of theory.

Atom	x	y	z
Li	0.000000	0.000000	1.000000
Ar	2.384609	0.000000	1.000000
Ar	−2.384609	0.000000	1.000000

Table A3: Cartesian coordinates in Angstroms (Å) for the D_{3h} optimized geometry of Li^+Ar_3 at the MP2/TZ level of theory.

Atom	x	y	z
Li	0.000000	0.000000	0.000000
Ar	0.000000	0.000000	2.394944
Ar	2.074082	0.000000	−1.197472
Ar	−2.074082	0.000000	−1.197472

Table A4: Cartesian coordinates in Angstroms (Å) for the T_d optimized geometry of Li^+Ar_4 at the MP2/TZ level of theory.

Atom	x	y	z
Li	0.000000	0.000000	0.000000
Ar	0.000000	0.000000	2.412869
Ar	2.274875	0.000000	−0.804290
Ar	−1.137438	1.970100	−0.804290
Ar	−1.137438	−1.970100	−0.804290

Table A5: Cartesian coordinates in Angstroms (Å) for the C_{4v} optimized geometry of Li^+Ar_5 at the MP2/TZ level of theory.

Atom	x	y	z
Li	0.000000	0.000000	0.015788
Ar	0.000000	0.000000	2.472712
Ar	2.497616	0.000000	−0.364412
Ar	0.000000	−2.497616	−0.364412
Ar	−2.497616	0.000000	−0.364412
Ar	0.000000	2.497616	−0.364412

Table A6: Cartesian coordinates in Angstroms (Å) for the D_{3h} optimized geometry of Li^+Ar_5 at the MP2/TZ level of theory.

Atom	x	y	z
Li	0.000000	0.000000	0.000000
Ar	0.000000	0.000000	2.476346
Ar	2.144579	0.000000	−1.238173
Ar	−2.144579	0.000000	−1.238173
Ar	0.000000	−2.567412	0.000000
Ar	0.000000	2.567412	0.000000

Table A7: Cartesian coordinates in Angstroms (Å) for the O_h optimized geometry of Li^+Ar_6 at the MP2/TZ level of theory.

Atom	x	y	z
Li	0.000000	0.000000	0.000000
Ar	0.000000	0.000000	2.556729
Ar	2.556729	0.000000	0.000000
Ar	0.000000	−2.556729	0.000000
Ar	0.000000	0.000000	−2.556729
Ar	−2.556729	0.000000	0.000000
Ar	0.000000	2.556729	0.000000

Table A8: Cartesian coordinates in Angstroms (Å) for the $C_{\infty v}$ optimized geometry of Na^+Ar at the MP2/TZ level of theory.

Atom	x	y	z
Na	0.000000	0.000000	−0.027051
Ar	0.000000	0.000000	2.777051

Table A9: Cartesian coordinates in Angstroms (Å) for the $D_{\infty h}$ optimized geometry of Na^+Ar_2 at the MP2/TZ level of theory.

Atom	x	y	z
Na	0.000000	0.000000	1.000000
Ar	2.807729	0.000000	1.000000
Ar	−2.807726	0.000000	1.000000

Table A10: Cartesian coordinates in Angstroms (Å) for the C_{2v} optimized geometry of Na^+Ar_2 at the MP2/TZ level of theory.

Atom	x	y	z
Na	0.004399	0.000000	0.004107
Ar	−0.030124	0.000000	2.815045
Ar	2.806358	0.000000	−0.223023

Table A11: Cartesian coordinates in Angstroms (Å) for the C_{3v} optimized geometry of Na^+Ar_3 at the MP2/TZ level of theory.

Atom	x	y	z
Na	0.000000	0.000000	1.016733
Ar	2.358536	0.000000	2.558112
Ar	−1.179268	2.042552	2.558112
Ar	−1.179268	−2.042552	2.558112

Table A12: Cartesian coordinates in Angstroms (Å) for the C_{2v} optimized geometry of Na^+Ar_3 at the MP2/TZ level of theory.

Atom	x	y	z
Na	0.000000	0.000000	0.011514
Ar	0.000000	0.000000	2.831406
Ar	2.809369	0.000000	−0.156101
Ar	−2.809369	0.000000	−0.156101

Table A13: Cartesian coordinates in Angstroms (Å) for the C_{2v} optimized geometry of Na^+Ar_4 at the MP2/TZ level of theory.

Atom	x	y	z
Na	0.000000	0.000000	1.020576
Ar	2.815286	0.000000	0.869600
Ar	−2.815286	0.000000	0.869600
Ar	0.000000	1.998616	3.018229
Ar	0.000000	−1.998616	3.018229

Table A14: Cartesian coordinates in Angstroms (Å) for the T_d optimized geometry of Na^+Ar_4 at the MP2/TZ level of theory.

Atom	x	y	z
Na	0.000000	0.000000	0.000000
Ar	0.000000	0.000000	2.808741
Ar	2.648106	0.000000	−0.936247
Ar	−1.324053	2.293327	−0.936247
Ar	−1.324053	−2.293327	−0.936247

Table A15: Cartesian coordinates in Angstroms (Å) for the C_{4v} optimized geometry of Na^+Ar_5 at the MP2/TZ level of theory.

Atom	x	y	z
Na	0.000000	0.000000	0.024049
Ar	0.000000	0.000000	2.855356
Ar	2.827867	0.000000	−0.004099
Ar	0.000000	−2.827867	−0.004099
Ar	−2.827867	0.000000	−0.004099
Ar	0.000000	2.827867	−0.004099

Table A16: Cartesian coordinates in Angstroms (Å) for the D_{3h} optimized geometry of Na^+Ar_5 at the MP2/TZ level of theory.

Atom	x	y	z
Na	0.000000	0.000000	0.000000
Ar	0.000000	0.000000	2.822346
Ar	2.444224	0.000000	−1.411173
Ar	−2.444224	0.000000	−1.411173
Ar	0.000000	2.831448	0.000000
Ar	0.000000	−2.831448	0.000000

Table A17: Cartesian coordinates in Angstroms (Å) for the O_h optimized geometry of Na^+Ar_6 at the MP2/TZ level of theory.

Atom	x	y	z
Na	0.000000	0.000000	0.000000
Ar	0.000000	0.000000	2.831735
Ar	2.831735	0.000000	0.000000
Ar	0.000000	−2.831735	0.000000
Ar	0.000000	0.000000	−2.831735
Ar	−2.831735	0.000000	0.000000
Ar	0.000000	2.831735	0.000000

Table A18: Cartesian coordinates in Angstroms (Å) for the $C_{\infty v}$ optimized geometry of K^+Ar at the MP2/TZ level of theory.

Atom	x	y	z
K	0.000000	0.000000	−0.006573
Ar	0.000000	0.000000	3.206573

Table A19: Cartesian coordinates in Angstroms (Å) for the C_{2v} optimized geometry of K^+Ar_2 at the MP2/TZ level of theory.

Atom	x	y	z
K	−0.007392	0.000000	−0.009626
Ar	−0.009426	0.000000	3.209426
Ar	3.103197	0.000000	0.819198

Table A20: Cartesian coordinates in Angstroms (Å) for the $D_{\infty h}$ optimized geometry of K^+Ar_2 at the MP2/TZ level of theory.

Atom	x	y	z
K	0.000000	0.000000	1.000000
Ar	3.221236	0.000000	1.000000
Ar	−3.221236	0.000000	1.000000

Table A21: Cartesian coordinates in Angstroms (Å) for the C_{3v} optimized geometry of K^+Ar_3 at the MP2/TZ level of theory.

Atom	x	y	z
K	0.000000	0.000000	1.706490
Ar	0.000000	2.251202	−0.600185
Ar	1.949598	−1.125601	−0.600185
Ar	−1.949598	−1.125601	−0.600185

Table A22: Cartesian coordinates in Angstroms (Å) for the C_{2v} optimized geometry of K^+Ar_3 at the MP2/TZ level of theory.

Atom	x	y	z
K	0.000000	0.000000	0.001025
Ar	0.000000	0.000000	3.224089
Ar	3.118731	0.000000	0.819586
Ar	−3.118731	0.000000	0.819586

Table A23: Cartesian coordinates in Angstroms (Å) for the C_{2v} optimized geometry of K^+Ar_4 at the MP2/TZ level of theory.

Atom	x	y	z
K	0.000000	0.000000	0.397933
Ar	3.032517	0.000000	1.505858
Ar	−3.032517	0.000000	1.505858
Ar	0.000000	1.939030	2.977594
Ar	0.000000	−1.939030	2.977594

Table A24: Cartesian coordinates in Angstroms (Å) for the T_d optimized geometry of K^+Ar_4 at the MP2/TZ level of theory.

Atom	x	y	z
K	0.000000	0.000000	0.000000
Ar	0.000000	0.000000	3.218048
Ar	3.034004	0.000000	−1.072683
Ar	−1.517002	2.627525	−1.072683
Ar	−1.517002	−2.627525	−1.072683

Table A25: Cartesian coordinates in Angstroms (Å) for the C_{4v} optimized geometry of K^+Ar_5 at the MP2/TZ level of theory.

Atom	x	y	z
K	0.000000	0.000000	−0.010102
Ar	0.000000	0.000000	3.248313
Ar	3.059109	0.000000	0.978474
Ar	0.000000	−3.059109	0.978474
Ar	−3.059109	0.000000	0.978474
Ar	0.000000	3.059109	0.978474

Table A26: Cartesian coordinates in Angstroms (Å) for the D_{3h} optimized geometry of K^+Ar_5 at the MP2/TZ level of theory.

Atom	x	y	z
K	0.000000	0.000000	0.000000
Ar	0.000000	3.208957	0.000000
Ar	−2.779038	−1.604479	0.000000
Ar	2.779038	−1.604479	0.000000
Ar	0.000000	0.000000	3.207295
Ar	0.000000	0.000000	−3.207295

Table A27: Cartesian coordinates in Angstroms (Å) for the C_{2v} optimized geometry of K^+Ar_6 at the MP2/TZ level of theory.

Atom	x	y	z
K	−0.615687	−0.425669	0.000000
Ar	0.464922	2.628839	0.000000
Ar	2.623638	−0.493238	0.000000
Ar	0.239735	0.165662	3.038227
Ar	−3.195475	1.502579	0.000000
Ar	0.239735	0.165662	−3.038227
Ar	0.277371	−3.520156	0.000000

Table A28: Cartesian coordinates in Angstroms (Å) for the O_h optimized geometry of K^+Ar_6 at the MP2/TZ level of theory.

Atom	x	y	z
K	0.000000	0.000000	0.000000
Ar	0.000000	0.000000	3.199324
Ar	3.199324	0.000000	0.000000
Ar	0.000000	−3.199325	0.000000
Ar	0.000000	0.000000	−3.199325
Ar	−3.199325	0.000000	0.000000
Ar	0.000000	3.199325	0.000000

Table A29: Cartesian coordinates in Angstroms (Å) for the $C_{\infty v}$ optimized geometry of Rb^+Ar at the MP2/TZ level of theory.

Atom	x	y	z
Rb	0.000000	0.000000	0.005455
Ar	0.000000	0.000000	3.394545

Table A30: Cartesian coordinates in Angstroms (Å) for the C_{2v} optimized geometry of Rb^+Ar_2 at the MP2/TZ level of theory.

Atom	x	y	z
Rb	−0.011297	0.000000	−0.016134
Ar	−0.000976	0.000000	3.378425
Ar	3.174962	0.000000	1.154718

Table A31: Cartesian coordinates in Angstroms (Å) for the $D_{\infty h}$ optimized geometry of Rb^+Ar_2 at the MP2/TZ level of theory.

Atom	x	y	z
Rb	0.000000	0.000000	1.000000
Ar	3.403856	0.000000	1.000000
Ar	−3.403856	0.000000	1.000000

Table A32: Cartesian coordinates in Angstroms (Å) for the C_{3v} optimized geometry of Rb^+Ar_3 at the MP2/TZ level of theory.

Atom	x	y	z
Rb	0.000000	0.000000	1.526745
Ar	0.000000	2.228485	−1.038695
Ar	1.929924	−1.114242	−1.038695
Ar	−1.929924	−1.114242	−1.038695

Table A33: Cartesian coordinates in Angstroms (Å) for the C_{2v} optimized geometry of Rb^+Ar_3 at the MP2/TZ level of theory.

Atom	x	y	z
Rb	0.000000	0.000000	−0.015483
Ar	0.000000	0.000000	3.384730
Ar	3.184349	0.000000	1.181727
Ar	−3.184349	0.000000	1.181727

Table A34: Cartesian coordinates in Angstroms (Å) for the C_{2v} optimized geometry of Rb^+Ar_4 at the MP2/TZ level of theory.

Atom	x	y	z
Rb	0.000000	0.000000	0.308164
Ar	3.060338	0.000000	1.799589
Ar	−3.060338	0.000000	1.799589
Ar	0.000000	1.923838	3.114313
Ar	0.000000	−1.923838	3.114313

Table A35: Cartesian coordinates in Angstroms (Å) for the T_d optimized geometry of Rb^+Ar_4 at the MP2/TZ level of theory.

Atom	x	y	z
Rb	0.000000	0.000000	0.000000
Ar	0.000000	0.000000	3.397008
Ar	3.202730	0.000000	−1.132336
Ar	−1.601365	2.773645	−1.132336
Ar	−1.601365	−2.773645	−1.132336

Table A36: Cartesian coordinates in Angstroms (Å) for the C_{4v} optimized geometry of Rb^+Ar_5 at the MP2/TZ level of theory.

Atom	x	y	z
Rb	0.000000	0.000000	−0.021304
Ar	0.000000	0.000000	3.431909
Ar	3.113014	0.000000	1.318763
Ar	0.000000	−3.113014	1.318764
Ar	−3.113014	0.000000	1.318764
Ar	0.000000	3.113014	1.318764

Table A37: Cartesian coordinates in Angstroms (Å) for the D_{3h} optimized geometry of Rb^+Ar_5 at the MP2/TZ level of theory.

Atom	x	y	z
Rb	0.000000	0.000000	0.000000
Ar	0.000000	3.388258	0.000000
Ar	−2.934317	−1.694129	0.000000
Ar	2.934317	−1.694129	0.000000
Ar	0.000000	0.000000	3.390825
Ar	0.000000	0.000000	−3.390825

Table A38: Cartesian coordinates in Angstroms (Å) for the C_{2v} optimized geometry of Rb^+Ar_6 at the MP2/TZ level of theory.

Atom	x	y	z
Rb	−0.760503	−0.489424	0.000000
Ar	0.616913	2.639683	0.000000
Ar	2.658086	−0.531895	0.000000
Ar	0.460079	0.295991	3.065383
Ar	−3.129666	1.958963	0.000000
Ar	0.460079	0.295991	−3.065383
Ar	0.486342	−3.660027	0.000000

Table A39: Cartesian coordinates in Angstroms (Å) for the O_h optimized geometry of Rb^+Ar_6 at the MP2/TZ level of theory.

Atom	x	y	z
Rb	0.000000	0.000000	0.000000
Ar	0.000000	0.000000	3.384149
Ar	3.384149	0.000000	0.000000
Ar	0.000000	−3.384149	0.000000
Ar	0.000000	0.000000	−3.384149
Ar	−3.384149	0.000000	0.000000
Ar	0.000000	3.384149	0.000000

Table A40: Cartesian coordinates in Angstroms (Å) for the $C_{\infty v}$ optimized geometry of $H^{-}Ar$ at the MP2/TZ level of theory.

Atom	x	y	z
H	0.000000	0.000000	−0.012741
Ar	0.000000	0.000000	3.727181

Table A41: Cartesian coordinates in Angstroms (Å) for the C_{2v} optimized geometry of $H^{-}Ar_2$ at the MP2/TZ level of theory.

Atom	x	y	z
H	0.009079	0.000000	−0.015737
Ar	−0.000290	0.000000	3.738022
Ar	3.236142	0.000000	1.870880

Table A42: Cartesian coordinates in Angstroms (Å) for the $D_{\infty h}$ optimized geometry of $H^{-}Ar_2$ at the MP2/TZ level of theory.

Atom	x	y	z
H	0.000000	0.000000	1.000000
Ar	3.738295	0.000000	1.000000
Ar	−3.738295	0.000000	1.000000

Table A43: Cartesian coordinates in Angstroms (Å) for the C_{3v} optimized geometry of H^-Ar_3 at the MP2/TZ level of theory.

Atom	x	y	z
H	0.000000	0.000000	0.979194
Ar	2.154916	0.000000	4.063950
Ar	−1.077458	1.866212	4.063950
Ar	−1.077458	−1.866212	4.063950

Table A44: Cartesian coordinates in Angstroms (Å) for the C_{2v} optimized geometry of H^-Ar_3 at the MP2/TZ level of theory.

Atom	x	y	z
H	0.000000	0.000000	−2.474021
Ar	0.000000	0.000000	1.294470
Ar	0.000000	3.233580	−0.569047
Ar	0.000000	−3.233580	−0.569047

Table A45: Cartesian coordinates in Angstroms (Å) for the C_{2v} optimized geometry of H^-Ar_4 at the MP2/TZ level of theory.

Atom	x	y	z
H	0.000000	0.000000	2.701658
Ar	0.000000	1.864589	−0.578592
Ar	0.000000	−1.864589	−0.578592
Ar	−3.045302	0.000000	0.493165
Ar	3.045302	0.000000	0.493165

Table A46: Cartesian coordinates in Angstroms (Å) for the T_d optimized geometry of H^-Ar_4 at the MP2/TZ level of theory.

Atom	x	y	z
H	0.000000	0.000000	0.000000
Ar	0.000000	0.000000	3.737499
Ar	3.523748	0.000000	−1.245833
Ar	−1.761874	−3.051656	−1.245833
Ar	−1.761874	3.051656	−1.245833

Table A47: Cartesian coordinates in Angstroms (Å) for the C_{4v} optimized geometry of H^-Ar_5 at the MP2/TZ level of theory.

Atom	x	y	z
H	0.000000	0.000000	−0.029576
Ar	0.000000	0.000000	5.219442
Ar	2.644158	0.000000	2.603683
Ar	0.000000	−2.644158	2.603683
Ar	−2.644158	0.000000	2.603683
Ar	0.000000	2.644158	2.603683

Table A48: Cartesian coordinates in Angstroms (Å) for the D_{3h} optimized geometry of H^-Ar_5 at the MP2/TZ level of theory.

Atom	x	y	z
H	0.000000	0.000000	0.000000
Ar	0.000000	0.000000	3.711287
Ar	3.214069	0.000000	−1.855643
Ar	−3.214069	0.000000	−1.855643
Ar	0.000000	3.698464	0.000000
Ar	0.000000	−3.698464	0.000000

Table A49: Cartesian coordinates in Angstroms (Å) for the C_{2v} optimized geometry of H^-Ar_6 at the MP2/TZ level of theory.

Atom	x	y	z
H	−1.590078	−1.014016	0.000000
Ar	0.252526	2.350428	0.000000
Ar	2.237456	−0.763151	0.000000
Ar	0.249619	0.159069	3.014071
Ar	−3.444383	2.222307	0.000000
Ar	0.249619	0.159069	−3.014071
Ar	0.561544	−4.060811	0.000000

Table A50: Cartesian coordinates in Angstroms (Å) for the O_h optimized geometry of H^-Ar_6 at the MP2/TZ level of theory.

Atom	x	y	z
H	0.000000	0.000000	0.000000
Ar	0.000000	0.000000	3.683672
Ar	3.683678	0.000000	0.000000
Ar	0.000000	−3.683672	0.000000
Ar	0.000000	0.000000	−3.683672
Ar	−3.683678	0.000000	0.000000
Ar	0.000000	3.683672	0.000000

Table A51: Cartesian coordinates in Angstroms (Å) for the $C_{\infty v}$ optimized geometry of F^-Ar at the MP2/TZ level of theory.

Atom	x	y	z
F	0.000000	0.000000	−0.038012
Ar	0.000000	0.000000	3.038012

Table A52: Cartesian coordinates in Angstroms (Å) for the C_{2v} optimized geometry of F^-Ar_2 at the MP2/TZ level of theory.

Atom	x	y	z
F	−0.007120	0.000000	−0.009320
Ar	0.000911	0.000000	3.079929
Ar	2.971294	0.000000	0.810786

Table A53: Cartesian coordinates in Angstroms (Å) for the $D_{\infty h}$ optimized geometry of F^-Ar_2 at the MP2/TZ level of theory.

Atom	x	y	z
F	0.000000	0.000000	0.000000
Ar	0.000000	0.000000	3.079859
Ar	0.000000	0.000000	−3.079859

Table A54: Cartesian coordinates in Angstroms (Å) for the C_{3v} optimized geometry of F^-Ar_3 at the MP2/TZ level of theory.

Atom	x	y	z
F	0.000000	0.000000	1.909902
Ar	0.000000	2.155537	−0.320356
Ar	−1.866749	−1.077768	−0.320356
Ar	1.866749	−1.077768	−0.320356

Table A55: Cartesian coordinates in Angstroms (Å) for the C_{2v} optimized geometry of F^-Ar_3 at the MP2/TZ level of theory.

Atom	x	y	z
F	0.000000	0.000000	−1.364923
Ar	0.000000	2.976022	−0.524958
Ar	0.000000	−2.976022	−0.524959
Ar	0.000000	0.000000	1.737455

Table A56: Cartesian coordinates in Angstroms (Å) for the C_{2v} optimized geometry of F^-Ar_4 at the MP2/TZ level of theory.

Atom	x	y	z
F	0.000000	0.000000	1.589342
Ar	0.000000	2.908328	0.505499
Ar	0.000000	−2.908328	0.505499
Ar	1.864215	0.000000	−0.905484
Ar	−1.864215	0.000000	−0.905484

Table A57: Cartesian coordinates in Angstroms (Å) for the T_d optimized geometry of F^-Ar_4 at the MP2/TZ level of theory.

Atom	x	y	z
F	0.000000	0.000000	0.000000
Ar	1.779152	1.779152	1.779152
Ar	−1.779152	−1.779152	1.779152
Ar	−1.779152	1.779152	−1.779152
Ar	1.779152	−1.779152	−1.779152

Table A58: Cartesian coordinates in Angstroms (Å) for the C_{4v} optimized geometry of F^-Ar_5 at the MP2/TZ level of theory.

Atom	x	y	z
F	0.000000	0.000000	−0.002781
Ar	0.000000	0.000000	3.171283
Ar	2.933010	0.000000	0.955509
Ar	0.000000	−2.933010	0.955509
Ar	−2.933010	0.000000	0.955509
Ar	0.000000	2.933010	0.955509

Table A59: Cartesian coordinates in Angstroms (Å) for the C_{4v} optimized geometry of F^-Ar_5 at the MP2/TZ level of theory.

Atom	x	y	z
F	0.000000	0.000000	0.000000
Ar	0.000000	0.000000	3.073423
Ar	2.661662	0.000000	−1.536711
Ar	−2.661662	0.000000	−1.536711
Ar	0.000000	3.069609	0.000000
Ar	0.000000	−3.069609	0.000000

Table A60: Cartesian coordinates in Angstroms (Å) for the C_{2v} optimized geometry of F^-Ar_6 at the MP2/TZ level of theory.

Atom	x	y	z
F	0.000055	0.780569	0.000000
Ar	1.844067	−1.750882	0.000000
Ar	−1.844369	−1.750575	0.000000
Ar	−0.000003	−0.240825	2.912618
Ar	2.916282	1.797461	0.000000
Ar	−0.000003	−0.240825	−2.912618
Ar	−2.916008	1.797935	0.000000

Table A61: Cartesian coordinates in Angstroms (Å) for the O_h optimized geometry of F^-Ar_6 at the MP2/TZ level of theory.

Atom	x	y	z
F	0.000000	0.000000	0.000000
Ar	0.000000	0.000000	3.059313
Ar	0.000000	3.059313	0.000000
Ar	3.059313	0.000000	0.000000
Ar	0.000000	0.000000	−3.059313
Ar	0.000000	−3.059313	0.000000
Ar	−3.059313	0.000000	0.000000

Table A62: Cartesian coordinates in Angstroms (Å) for the $C_{\infty v}$ optimized geometry of $Cl^{-}Ar$ at the MP2/TZ level of theory.

Atom	x	y	z
Cl	0.000000	0.000000	0.004742
Ar	0.000000	0.000000	3.695257

Table A63: Cartesian coordinates in Angstroms (Å) for the C_{2v} optimized geometry of $Cl^{-}Ar_2$ at the MP2/TZ level of theory.

Atom	x	y	z
Cl	−0.007704	0.000000	−0.013063
Ar	−0.000915	0.000000	3.682247
Ar	3.222837	0.000000	1.781085

Table A64: Cartesian coordinates in Angstroms (Å) for the $D_{\infty h}$ optimized geometry of $Cl^{-}Ar_2$ at the MP2/TZ level of theory.

Atom	x	y	z
Cl	0.000000	0.000000	0.000000
Ar	0.000000	0.000000	3.690739
Ar	0.000000	0.000000	−3.690739

Table A65: Cartesian coordinates in Angstroms (Å) for the C_{3v} optimized geometry of $Cl^{-}Ar_3$ at the MP2/TZ level of theory.

Atom	x	y	z
Cl	0.000000	0.000000	2.285035
Ar	0.000000	2.158194	−0.719653
Ar	−1.869051	−1.079097	−0.719653
Ar	1.869051	−1.079097	−0.719653

Table A66: Cartesian coordinates in Angstroms (Å) for the C_{2v} optimized geometry of $Cl^{-}Ar_3$ at the MP2/TZ level of theory.

Atom	x	y	z
Cl	0.000000	0.000000	−1.854527
Ar	0.000000	3.222753	−0.047271
Ar	0.000000	−3.222753	−0.047271
Ar	0.000000	0.000000	1.846892

Table A67: Cartesian coordinates in Angstroms (Å) for the C_{2v} optimized geometry of $Cl^{-}Ar_4$ at the MP2/TZ level of theory.

Atom	x	y	z
Cl	0.000000	0.000000	2.145259
Ar	0.000000	3.041642	0.040674
Ar	0.000000	−3.041642	0.040674
Ar	1.867462	0.000000	−1.054134
Ar	−1.867462	0.000000	−1.054134

Table A68: Cartesian coordinates in Angstroms (Å) for the T_d optimized geometry of Cl^-Ar_4 at the MP2/TZ level of theory.

Atom	x	y	z
Cl	0.000000	0.000000	0.000000
Ar	2.127553	2.127553	2.127553
Ar	−2.127553	−2.127553	2.127553
Ar	−2.127553	2.127553	−2.127553
Ar	2.127553	−2.127553	−2.127553

Table A69: Cartesian coordinates in Angstroms (Å) for the C_{4v} optimized geometry of Cl^-Ar_5 at the MP2/TZ level of theory.

Atom	x	y	z
Cl	0.000000	0.000000	−0.008850
Ar	0.000000	0.000000	3.803702
Ar	3.132409	0.000000	1.902820
Ar	0.000000	−3.132409	1.902820
Ar	−3.132409	0.000000	1.902820
Ar	0.000000	3.132409	1.902820

Table A70: Cartesian coordinates in Angstroms (Å) for the D_{3h} optimized geometry of $Cl^{-}Ar_5$ at the MP2/TZ level of theory.

Atom	x	y	z
Cl	0.000000	0.000000	0.000000
Ar	0.000000	0.000000	3.674818
Ar	3.182486	0.000000	−1.837409
Ar	−3.182486	0.000000	−1.837409
Ar	0.000000	3.671825	0.000000
Ar	0.000000	−3.671825	0.000000

Table A71: Cartesian coordinates in Angstroms (Å) for the C_{2v} optimized geometry of $Cl^{-}Ar_6$ at the MP2/TZ level of theory.

Atom	x	y	z
Cl	−0.000037	1.535598	0.000000
Ar	1.848561	−1.697502	0.000000
Ar	−1.848572	−1.697142	0.000000
Ar	0.000242	−0.552199	3.034194
Ar	3.685278	1.523803	0.000000
Ar	0.000242	−0.552199	−3.034194
Ar	−3.685453	1.523818	0.000000

Table A72: Cartesian coordinates in Angstroms (Å) for the O_h optimized geometry of Cl^-Ar_6 at the MP2/TZ level of theory.

Atom	x	y	z
Cl	0.000000	0.000000	0.000000
Ar	0.000000	0.000000	3.662366
Ar	0.000000	3.662366	0.000000
Ar	3.662366	0.000000	0.000000
Ar	0.000000	0.000000	−3.662366
Ar	0.000000	−3.662366	0.000000
Ar	−3.662366	0.000000	0.000000

Table A73: Cartesian coordinates in Angstroms (Å) for the $C_{\infty v}$ optimized geometry of Br^-Ar at the MP2/TZ level of theory.

Atom	x	y	z
Br	0.000000	0.000000	−0.015204
Ar	0.000000	0.000000	3.885802

Table A74: Cartesian coordinates in Angstroms (Å) for the C_{2v} optimized geometry of Br^-Ar_2 at the MP2/TZ level of theory.

Atom	x	y	z
Br	−0.009334	0.000000	−0.016986
Ar	−0.000711	0.000000	3.887285
Ar	3.281718	0.000000	2.083583

Table A75: Cartesian coordinates in Angstroms (Å) for the $D_{\infty h}$ optimized geometry of $Br^{-}Ar_2$ at the MP2/TZ level of theory.

Atom	x	y	z
Br	0.000000	0.000000	0.000000
Ar	0.000000	0.000000	3.900989
Ar	0.000000	0.000000	−3.900989

Table A76: Cartesian coordinates in Angstroms (Å) for the C_{3v} optimized geometry of $Br^{-}Ar_3$ at the MP2/TZ level of theory.

Atom	x	y	z
Br	0.000000	0.000000	1.979030
Ar	0.000000	2.159789	−1.276341
Ar	−1.870433	−1.079895	−1.276341
Ar	1.870433	−1.079895	−1.276341

Table A77: Cartesian coordinates in Angstroms (Å) for the C_{2v} optimized geometry of $Br^{-}Ar_3$ at the MP2/TZ level of theory.

Atom	x	y	z
Br	0.000000	0.000000	1.649602
Ar	0.000000	3.281187	−0.464056
Ar	0.000000	−3.281187	−0.464056
Ar	0.000000	0.000000	−2.259761

Table A78: Cartesian coordinates in Angstroms (Å) for the C_{2v} optimized geometry of $Br^{-}Ar_4$ at the MP2/TZ level of theory.

Atom	x	y	z
Br	0.000000	0.000000	1.970974
Ar	0.000000	3.069522	−0.443314
Ar	0.000000	−3.069522	−0.443314
Ar	1.869223	0.000000	−1.463424
Ar	−1.869223	0.000000	−1.463424

Table A79: Cartesian coordinates in Angstroms (Å) for the T_d optimized geometry of $Br^{-}Ar_4$ at the MP2/TZ level of theory.

Atom	x	y	z
Br	0.000000	0.000000	0.000000
Ar	2.247405	2.247405	2.247405
Ar	−2.247405	−2.247405	2.247405
Ar	−2.247405	2.247405	−2.247405
Ar	2.247405	−2.247405	−2.247405

Table A80: Cartesian coordinates in Angstroms (Å) for the C_{4v} optimized geometry of $Br^{-}Ar_5$ at the MP2/TZ level of theory.

Atom	x	y	z
Br	0.000000	0.000000	−0.015411
Ar	0.000000	0.000000	4.029549
Ar	3.175396	0.000000	2.198732
Ar	0.000000	−3.175396	2.198732
Ar	−3.175396	0.000000	2.198732
Ar	0.000000	3.175396	2.198732

Table A81: Cartesian coordinates in Angstroms (Å) for the D_{3h} optimized geometry of $Br^{-}Ar_5$ at the MP2/TZ level of theory.

Atom	x	y	z
Br	0.000000	0.000000	0.000000
Ar	0.000000	0.000000	3.883000
Ar	3.362777	0.000000	−1.941500
Ar	−3.362777	0.000000	−1.941500
Ar	0.000000	3.881781	0.000000
Ar	0.000000	−3.881781	0.000000

Table A82: Cartesian coordinates in Angstroms (Å) for the C_{2v} optimized geometry of $Br^{-}Ar_6$ at the MP2/TZ level of theory.

Atom	x	y	z
Br	−1.385770	0.732428	0.000000
Ar	2.544067	0.749336	0.000000
Ar	0.814598	−2.524073	0.000000
Ar	0.732994	−0.387675	3.060530
Ar	0.738645	3.992603	0.000000
Ar	0.732994	−0.387675	−3.060530
Ar	−2.882219	−2.859414	0.000000

Table A83: Cartesian coordinates in Angstroms (Å) for the O_h optimized geometry of $Br^{-}Ar_6$ at the MP2/TZ level of theory.

Atom	x	y	z
Br	0.000000	0.000000	0.000000
Ar	0.000000	0.000000	3.872743
Ar	0.000000	3.872743	0.000000
Ar	3.872743	0.000000	0.000000
Ar	0.000000	0.000000	−3.872743
Ar	0.000000	−3.872743	0.000000
Ar	−3.872743	0.000000	0.000000

Table A84: Cartesian coordinates in Angstroms (Å) for the $C_{\infty v}$ optimized geometry of Li^+Ar at the MP2/QZ level of theory.

Atom	x	y	z
Li	0.000000	0.000000	0.018680
Ar	0.000000	0.000000	2.381320

Table A85: Cartesian coordinates in Angstroms (Å) for the $D_{\infty h}$ optimized geometry of Li^+Ar_2 at the MP2/QZ level of theory.

Atom	x	y	z
Li	0.000000	0.000000	1.000000
Ar	2.373307	0.000000	1.000000
Ar	−2.373307	0.000000	1.000000

Table A86: Cartesian coordinates in Angstroms (Å) for the D_{3h} optimized geometry of Li^+Ar_3 at the MP2/QZ level of theory.

Atom	x	y	z
Li	0.000000	0.000000	0.000000
Ar	0.000000	0.000000	2.382258
Ar	2.063096	0.000000	−1.191129
Ar	−2.063096	0.000000	−1.191129

Table A87: Cartesian coordinates in Angstroms (Å) for the T_d optimized geometry of Li^+Ar_4 at the MP2/QZ level of theory.

Atom	x	y	z
Li	0.000000	0.000000	0.000000
Ar	0.000000	0.000000	2.401562
Ar	2.264214	0.000000	−0.800521
Ar	−1.132107	1.960867	−0.800521
Ar	−1.132107	−1.960867	−0.800521

Table A88: Cartesian coordinates in Angstroms (Å) for the C_{4v} optimized geometry of Li^+Ar_5 at the MP2/QZ level of theory.

Atom	x	y	z
Li	0.000000	0.000000	0.016540
Ar	0.000000	0.000000	2.431360
Ar	2.489103	0.000000	−0.370815
Ar	0.000000	−2.489103	−0.370815
Ar	−2.489103	0.000000	−0.370815
Ar	0.000000	2.489103	−0.370815

Table A89: Cartesian coordinates in Angstroms (Å) for the D_{3h} optimized geometry of Li^+Ar_5 at the MP2/QZ level of theory.

Atom	x	y	z
Li	0.000000	0.000000	0.000000
Ar	0.000000	0.000000	2.466215
Ar	2.135804	0.000000	−1.233107
Ar	−2.135804	0.000000	−1.233107
Ar	0.000000	−2.552396	0.000000
Ar	0.000000	2.552396	0.000000

Table A90: Cartesian coordinates in Angstroms (Å) for the O_h optimized geometry of Li^+Ar_6 at the MP2/QZ level of theory.

Atom	x	y	z
Li	0.000000	0.000000	0.000000
Ar	0.000000	0.000000	2.546511
Ar	2.546511	0.000000	0.000000
Ar	0.000000	−2.546511	0.000000
Ar	0.000000	0.000000	−2.546511
Ar	−2.546511	0.000000	0.000000
Ar	0.000000	2.546511	0.000000

Table A91: Cartesian coordinates in Angstroms (Å) for the $C_{\infty v}$ optimized geometry of Na^+Ar at the MP2/QZ level of theory.

Atom	x	y	z
Na	0.000000	0.000000	−0.013776
Ar	0.000000	0.000000	2.763776

Table A92: Cartesian coordinates in Angstroms (Å) for the $D_{\infty h}$ optimized geometry of Na^+Ar_2 at the MP2/QZ level of theory.

Atom	x	y	z
Na	0.000000	0.000000	1.000000
Ar	2.784105	0.000000	1.000000
Ar	−2.784105	0.000000	1.000000

Table A93: Cartesian coordinates in Angstroms (Å) for the C_{2v} optimized geometry of Na^+Ar_2 at the MP2/QZ level of theory.

Atom	x	y	z
Na	−0.004490	0.000000	−0.004090
Ar	0.029715	0.000000	2.782890
Ar	2.773589	0.000000	−0.229261

Table A94: Cartesian coordinates in Angstroms (Å) for the C_{3v} optimized geometry of Na^+Ar_3 at the MP2/QZ level of theory.

Atom	x	y	z
Na	0.000000	0.000000	0.983292
Ar	2.318653	0.000000	2.546976
Ar	−1.159326	2.008012	2.546976
Ar	−1.159326	−2.008012	2.546976

Table A95: Cartesian coordinates in Angstroms (Å) for the C_{2v} optimized geometry of Na^+Ar_3 at the MP2/QZ level of theory.

Atom	x	y	z
Na	0.000000	0.000000	−0.011501
Ar	0.000000	0.000000	2.785828
Ar	2.789765	0.000000	−0.144807
Ar	−2.789765	0.000000	−0.144807

Table A96: Cartesian coordinates in Angstroms (Å) for the C_{4v} optimized geometry of Na^+Ar_4 at the MP2/QZ level of theory.

Atom	x	y	z
Na	0.000000	0.000000	0.978889
Ar	2.799666	0.000000	0.893810
Ar	−2.799666	0.000000	0.893810
Ar	0.000000	1.985014	2.962096
Ar	0.000000	−1.985014	2.962096

Table A97: Cartesian coordinates in Angstroms (Å) for the T_d optimized geometry of Na^+Ar_4 at the MP2/QZ level of theory.

Atom	x	y	z
Na	0.000000	0.000000	0.000000
Ar	0.000000	0.000000	2.790509
Ar	2.630917	0.000000	−0.930170
Ar	−1.315458	2.278441	−0.930170
Ar	−1.315458	−2.278441	−0.930170

Table A98: Cartesian coordinates in Angstroms (Å) for the C_{4v} optimized geometry of Na^+Ar_5 at the MP2/QZ level of theory.

Atom	x	y	z
Na	0.000000	0.000000	−0.024041
Ar	0.000000	0.000000	2.790252
Ar	2.810511	0.000000	−0.011889
Ar	0.000000	−2.810511	−0.011889
Ar	−2.810511	0.000000	−0.011889
Ar	0.000000	2.810511	−0.011889

Table A99: Cartesian coordinates in Angstroms (Å) for the D_{3h} optimized geometry of Na^+Ar_5 at the MP2/QZ level of theory.

Atom	x	y	z
Na	0.000000	0.000000	0.000000
Ar	0.000000	0.000000	2.804003
Ar	2.428338	0.000000	−1.402001
Ar	−2.428338	0.000000	−1.402001
Ar	0.000000	2.812967	0.000000
Ar	0.000000	−2.812967	0.000000

Table A100: Cartesian coordinates in Angstroms (Å) for the O_h optimized geometry of Na^+Ar_6 at the MP2/QZ level of theory.

Atom	x	y	z
Na	0.000000	0.000000	0.000000
Ar	0.000000	0.000000	2.814139
Ar	2.814139	0.000000	0.000000
Ar	0.000000	−2.814139	0.000000
Ar	0.000000	0.000000	−2.814139
Ar	−2.814139	0.000000	0.000000
Ar	0.000000	2.814139	0.000000

Table A101: Cartesian coordinates in Angstroms (Å) for the $C_{\infty v}$ optimized geometry of K^+Ar at the MP2/QZ level of theory.

Atom	x	y	z
K	0.000000	0.000000	0.005936
Ar	0.000000	0.000000	3.194064

Table A102: Cartesian coordinates in Angstroms (Å) for the C_{2v} optimized geometry of K^+Ar_2 at the MP2/QZ level of theory.

Atom	x	y	z
K	−0.182753	0.000000	−0.167462
Ar	0.370780	0.000000	2.978816
Ar	2.999796	0.000000	0.109748

Table A103: Cartesian coordinates in Angstroms (Å) for the $D_{\infty h}$ optimized geometry of K^+Ar_2 at the MP2/QZ level of theory.

Atom	x	y	z
K	0.000000	0.000000	1.000000
Ar	3.196734	0.000000	1.000000
Ar	−3.196734	0.000000	1.000000

Table A104: Cartesian coordinates in Angstroms (Å) for the C_{3v} optimized geometry of K^+Ar_3 at the MP2/QZ level of theory.

Atom	x	y	z
K	0.000000	0.000000	0.410157
Ar	2.235468	0.000000	−1.878752
Ar	−1.117734	−1.935972	−1.878752
Ar	−1.117734	1.935972	−1.878752

Table A105: Cartesian coordinates in Angstroms (Å) for the C_{2v} optimized geometry of K^+Ar_3 at the MP2/QZ level of theory.

Atom	x	y	z
K	0.000000	0.000000	−0.553021
Ar	0.000000	0.000000	2.647079
Ar	3.091287	0.000000	0.279072
Ar	−3.091287	0.000000	0.279072

Table A106: Cartesian coordinates in Angstroms (Å) for the C_{2v} optimized geometry of K^+Ar_4 at the MP2/QZ level of theory.

Atom	x	y	z
K	0.000000	0.000000	0.405071
Ar	3.009755	0.000000	1.509180
Ar	−3.009755	0.000000	1.509180
Ar	0.000000	1.930200	2.963234
Ar	0.000000	−1.930200	2.963234

Table A107: Cartesian coordinates in Angstroms (Å) for the T_d optimized geometry of K^+Ar_4 at the MP2/QZ level of theory.

Atom	x	y	z
K	0.000000	0.000000	0.000000
Ar	0.000000	0.000000	3.196694
Ar	3.013873	0.000000	−1.065565
Ar	−1.506936	2.610090	−1.065565
Ar	−1.506936	−2.610090	−1.065565

Table A108: Cartesian coordinates in Angstroms (Å) for the C_{4v} optimized geometry of K^+Ar_5 at the MP2/QZ level of theory.

Atom	x	y	z
K	0.000000	0.000000	−0.653189
Ar	0.000000	0.000000	2.583676
Ar	3.041106	0.000000	0.325623
Ar	0.000000	−3.041106	0.325623
Ar	−3.041106	0.000000	0.325623
Ar	0.000000	3.041106	0.325623

Table A109: Cartesian coordinates in Angstroms (Å) for the D_{3h} optimized geometry of K^+Ar_5 at the MP2/QZ level of theory.

Atom	x	y	z
K	0.000000	0.000000	0.000000
Ar	0.000000	0.000000	3.191000
Ar	2.763487	0.000000	−1.595500
Ar	−2.763487	0.000000	−1.595500
Ar	0.000000	3.187474	0.000000
Ar	0.000000	−3.187474	0.000000

Table A110: Cartesian coordinates in Angstroms (Å) for the C_{2v} optimized geometry of K^+Ar_6 at the MP2/QZ level of theory.

Atom	x	y	z
K	0.000036	0.810839	0.000000
Ar	1.892531	−1.795809	0.000000
Ar	−1.892798	−1.795876832	0.000000
Ar	−0.000265	−2.597215	3.012853
Ar	3.033505	1.841342	0.000000
Ar	−0.000069	−0.255972	−3.012853
Ar	−3.033404	1.841415	0.000000

Table A111: Cartesian coordinates in Angstroms (Å) for the O_h optimized geometry of K^+Ar_6 at the MP2/QZ level of theory.

Atom	x	y	z
K	0.000000	0.000000	0.000000
Ar	0.000000	0.000000	3.182039
Ar	3.182038	0.000000	0.000000
Ar	0.000000	−3.182038	0.000000
Ar	0.000000	0.000000	−3.182038
Ar	−3.182038	0.000000	0.000000
Ar	0.000000	3.182038	0.000000

Table A112: Cartesian coordinates in Angstroms (Å) for the $C_{\infty v}$ optimized geometry of Rb^+Ar at the MP2/QZ level of theory.

Atom	x	y	z
Rb	0.000000	0.000000	0.019739
Ar	0.000000	0.000000	3.380261

Table A113: Cartesian coordinates in Angstroms (Å) for the C_{2v} optimized geometry of Rb^+Ar_2 at the MP2/QZ level of theory.

Atom	x	y	z
Rb	−0.239417	0.000000	−0.219385
Ar	0.489133	0.000000	3.066537
Ar	3.097498	0.000000	0.220006

Table A114: Cartesian coordinates in Angstroms (Å) for the $D_{\infty h}$ optimized geometry of Rb^+Ar_2 at the MP2/QZ level of theory.

Atom	x	y	z
Rb	0.000000	0.000000	1.000000
Ar	3.372815	0.000000	1.000000
Ar	−3.372815	0.000000	1.000000

Table A115: Cartesian coordinates in Angstroms (Å) for the C_{3v} optimized geometry of Rb^+Ar_3 at the MP2/QZ level of theory.

Atom	x	y	z
Rb	0.000000	0.000000	0.277364
Ar	2.218132	0.000000	−2.260006
Ar	−1.109066	−1.920959	−2.260006
Ar	−1.109066	−1.920959	−2.260006

Table A116: Cartesian coordinates in Angstroms (Å) for the C_{2v} optimized geometry of Rb^+Ar_3 at the MP2/QZ level of theory.

Atom	x	y	z
Rb	0.000000	0.000000	−0.735033
Ar	0.000000	0.000000	2.637401
Ar	3.161303	0.000000	0.445101
Ar	−3.161303	0.000000	0.445101

Table A117: Cartesian coordinates in Angstroms (Å) for the C_{2v} optimized geometry of Rb^+Ar_4 at the MP2/QZ level of theory.

Atom	x	y	z
Rb	0.000000	0.000000	0.191072
Ar	3.042437	0.000000	1.658528
Ar	−3.042437	0.000000	1.658528
Ar	0.000000	1.916350	2.970027
Ar	0.000000	−1.916350	2.970027

Table A118: Cartesian coordinates in Angstroms (Å) for the T_d optimized geometry of Rb^+Ar_4 at the MP2/QZ level of theory.

Atom	x	y	z
Rb	0.000000	0.000000	0.000000
Ar	0.000000	0.000000	3.370392
Ar	3.177636	0.000000	−1.123464
Ar	−1.588818	2.751913	−1.123464
Ar	−1.588818	−2.751913	−1.123464

Table A119: Cartesian coordinates in Angstroms (Å) for the C_{4v} optimized geometry of Rb^+Ar_5 at the MP2/QZ level of theory.

Atom	x	y	z
Rb	0.000000	0.000000	−0.905666
Ar	0.000000	0.000000	2.516234
Ar	3.096806	0.000000	0.410279
Ar	0.000000	−3.096806	0.410279
Ar	−3.096806	0.000000	0.410279
Ar	0.000000	3.096806	0.410279

Table A120: Cartesian coordinates in Angstroms (Å) for the D_{3h} optimized geometry of Rb^+Ar_5 at the MP2/QZ level of theory.

Atom	x	y	z
Rb	0.000000	0.000000	0.000000
Ar	0.000000	0.000000	3.364234
Ar	2.913512	0.000000	−1.682117
Ar	−2.913512	0.000000	−1.682117
Ar	0.000000	3.364133	0.000000
Ar	0.000000	−3.364133	0.000000

Table A121: Cartesian coordinates in Angstroms (Å) for the C_{2v} optimized geometry of Rb^+Ar_6 at the MP2/QZ level of theory.

Atom	x	y	z
Rb	−0.000018	1.081684	0.000000
Ar	1.879591	−1.745878	0.000000
Ar	−1.880033	−1.745555	0.000000
Ar	0.000245	−0.365219	3.043011
Ar	3.309792	1.765212	0.000000
Ar	0.000245	−0.365220	−3.043011
Ar	−3.309914	1.765101	0.000000

Table A122: Cartesian coordinates in Angstroms (Å) for the O_h optimized geometry of Rb^+Ar_6 at the MP2/QZ level of theory.

Atom	x	y	z
Rb	0.000000	0.000000	0.000000
Ar	0.000000	0.000000	3.358967
Ar	3.358967	0.000000	0.000000
Ar	0.000000	−3.358967	0.000000
Ar	0.000000	0.000000	−3.358967
Ar	−3.358967	0.000000	0.000000
Ar	0.000000	3.358967	0.000000

Table A123: Cartesian coordinates in Angstroms (Å) for the $C_{\infty v}$ optimized geometry of H^-Ar at the MP2/QZ level of theory.

Atom	x	y	z
H	0.000000	0.000000	−0.012741
Ar	0.000000	0.000000	3.727181

Table A124: Cartesian coordinates in Angstroms (Å) for the C_{2v} optimized geometry of H^-Ar_2 at the MP2/QZ level of theory.

Atom	x	y	z
H	0.009130	0.000000	0.015914
Ar	0.000268	0.000000	3.743270
Ar	3.231458	0.000000	1.889378

Table A125: Cartesian coordinates in Angstroms (Å) for the $D_{\infty h}$ optimized geometry of H^-Ar_2 at the MP2/QZ level of theory.

Atom	x	y	z
H	0.000000	0.000000	1.000000
Ar	3.713437	0.000000	1.000000
Ar	−3.713437	0.000000	1.000000

Table A126: Cartesian coordinates in Angstroms (Å) for the C_{3v} optimized geometry of H^-Ar_3 at the MP2/QZ level of theory.

Atom	x	y	z
H	0.000000	0.000000	0.503130
Ar	2.147884	0.000000	3.560147
Ar	−1.073942	1.860122	3.560147
Ar	−1.073942	−1.860122	3.560147

Table A127: Cartesian coordinates in Angstroms (Å) for the C_{2v} optimized geometry of H^-Ar_3 at the MP2/QZ level of theory.

Atom	x	y	z
H	0.000000	0.000000	−2.148661
Ar	0.000000	0.000000	1.593187
Ar	0.000000	3.220679	−0.270455
Ar	0.000000	−3.220679	−0.270455

Table A128: Cartesian coordinates in Angstroms (Å) for the C_{2v} optimized geometry of H^-Ar_4 at the MP2/QZ level of theory.

Atom	x	y	z
H	0.000000	0.000000	2.675833
Ar	0.000000	1.858435	−0.577377
Ar	0.000000	−1.858435	−0.577377
Ar	−3.033788	0.000000	0.495303
Ar	3.033788	0.000000	0.495303

Table A129: Cartesian coordinates in Angstroms (Å) for the T_d optimized geometry of H^-Ar_4 at the MP2/QZ level of theory.

Atom	x	y	z
H	0.000000	0.000000	0.000000
Ar	0.000000	0.000000	3.716968
Ar	3.504391	0.000000	−1.238989
Ar	−1.752195	−3.034891	−1.238989
Ar	−1.752195	3.034891	−1.238989

Table A130: Cartesian coordinates in Angstroms (Å) for the C_{4v} optimized geometry of H^-Ar_5 at the MP2/QZ level of theory.

Atom	x	y	z
H	0.000000	0.000000	−2.120546
Ar	0.000000	0.000000	3.078505
Ar	2.638693	0.000000	0.480840
Ar	0.000000	−2.638693	0.480840
Ar	−2.638693	0.000000	0.480840
Ar	0.000000	2.638693	0.480840

Table A131: Cartesian coordinates in Angstroms (Å) for the D_{3h} optimized geometry of H^-Ar_5 at the MP2/QZ level of theory.

Atom	x	y	z
H	0.000000	0.000000	0.000000
Ar	0.000000	0.000000	3.693731
Ar	3.198865	0.000000	−1.846866
Ar	−3.198865	0.000000	−1.846866
Ar	0.000000	3.678744	0.000000
Ar	0.000000	−3.678744	0.000000

Table A132: Cartesian coordinates in Angstroms (Å) for the C_{2v} optimized geometry of H^-Ar_6 at the MP2/QZ level of theory.

Atom	x	y	z
H	1.571458	−1.002029	0.000000
Ar	−2.227621	−0.762287	0.000000
Ar	−0.249043	2.340827	0.000000
Ar	−0.249092	0.158615	3.004974
Ar	−0.547951	−4.044131	0.000000
Ar	−0.249092	0.158615	−3.004974
Ar	3.435070	2.203290	0.000000

Table A133: Cartesian coordinates in Angstroms (Å) for the O_h optimized geometry of H^-Ar_6 at the MP2/QZ level of theory.

Atom	x	y	z
H	0.000000	0.000000	0.000000
Ar	0.000000	0.000000	3.664807
Ar	3.664807	0.000000	0.000000
Ar	0.000000	−3.664807	0.000000
Ar	0.000000	0.000000	−3.664807
Ar	−3.664807	0.000000	0.000000
Ar	0.000000	3.664807	0.000000

Table A134: Cartesian coordinates in Angstroms (Å) for the $C_{\infty v}$ optimized geometry of F^-Ar at the MP2/QZ level of theory.

Atom	x	y	z
F	0.000000	0.000000	−0.029483
Ar	0.000000	0.000000	3.029483

Table A135: Cartesian coordinates in Angstroms (Å) for the C_{2v} optimized geometry of F^-Ar_2 at the MP2/QZ level of theory.

Atom	x	y	z
F	0.070729	0.000000	0.122507
Ar	−0.323869	0.000000	3.170315
Ar	2.907507	0.000000	1.304678

Table A136: Cartesian coordinates in Angstroms (Å) for the $D_{\infty h}$ optimized geometry of F^-Ar_2 at the MP2/QZ level of theory.

Atom	x	y	z
F	0.000000	0.000000	0.000000
Ar	0.000000	0.000000	3.065154
Ar	0.000000	0.000000	−3.065154

Table A137: Cartesian coordinates in Angstroms (Å) for the C_{3v} optimized geometry of F^-Ar_3 at the MP2/QZ level of theory.

Atom	x	y	z
F	0.000000	0.000000	1.897658
Ar	0.000000	2.150561	−0.316282
Ar	−1.862440	−1.075280	−0.316282
Ar	1.862440	−1.075280	−0.316282

Table A138: Cartesian coordinates in Angstroms (Å) for the C_{2v} optimized geometry of F^-Ar_3 at the MP2/QZ level of theory.

Atom	x	y	z
F	0.000000	0.000000	−1.351601
Ar	0.000000	2.964817	−0.525003
Ar	0.000000	−2.964817	−0.525003
Ar	0.000000	0.000000	1.736894

Table A139: Cartesian coordinates in Angstroms (Å) for the C_{2v} optimized geometry of F^-Ar_4 at the MP2/QZ level of theory.

Atom	x	y	z
F	0.000000	0.000000	1.577266
Ar	0.000000	2.898430	0.506518
Ar	0.000000	−2.898430	0.506518
Ar	1.859776	0.000000	−0.904179
Ar	−1.859776	0.000000	−0.904179

Table A140: Cartesian coordinates in Angstroms (Å) for the T_d optimized geometry of F^-Ar_4 at the MP2/QZ level of theory.

Atom	x	y	z
F	0.000000	0.000000	0.000000
Ar	1.771114	1.771114	1.771114
Ar	−1.771114	−1.771114	1.771114
Ar	−1.771114	1.771114	−1.771114
Ar	1.771114	−1.771114	−1.771114

Table A141: Cartesian coordinates in Angstroms (Å) for the C_{4v} optimized geometry of F^-Ar_5 at the MP2/QZ level of theory.

Atom	x	y	z
F	0.000000	0.000000	0.002702
Ar	0.000000	0.000000	3.168262
Ar	2.920060	0.000000	0.958944
Ar	0.000000	−2.920060	0.958944
Ar	−2.920060	0.000000	0.958944
Ar	0.000000	2.920060	0.958944

Table A142: Cartesian coordinates in Angstroms (Å) for the C_{4v} optimized geometry of F^-Ar_5 at the MP2/QZ level of theory.

Atom	x	y	z
F	0.000000	0.000000	0.000000
Ar	0.000000	0.000000	3.059248
Ar	2.649386	0.000000	−1.529624
Ar	−2.649386	0.000000	−1.529624
Ar	0.000000	3.056441	0.000000
Ar	0.000000	−3.056441	0.000000

Table A143: Cartesian coordinates in Angstroms (Å) for the C_{2v} optimized geometry of F^-Ar_6 at the MP2/QZ level of theory.

Atom	x	y	z
F	−0.000016	0.785322	0.000000
Ar	1.837216	−1.742241	0.000000
Ar	−1.837308	−1.742191	0.000000
Ar	0.000053	−0.243288	2.900437
Ar	2.910568	1.787836	0.000000
Ar	0.000053	−0.243288	−2.900437
Ar	−2.910569	1.787937	0.000000

Table A144: Cartesian coordinates in Angstroms (Å) for the O_h optimized geometry of F^-Ar_6 at the MP2/QZ level of theory.

Atom	x	y	z
F	0.000000	0.000000	0.000000
Ar	0.000000	0.000000	3.049842
Ar	0.000000	3.049842	0.000000
Ar	3.049842	0.000000	0.000000
Ar	0.000000	0.000000	−3.049842
Ar	0.000000	−3.049842	0.000000
Ar	−3.049842	0.000000	0.000000

Table A145: Cartesian coordinates in Angstroms (Å) for the $C_{\infty v}$ optimized geometry of $Cl^{-}Ar$ at the MP2/QZ level of theory.

Atom	x	y	z
Cl	0.000000	0.000000	0.016816
Ar	0.000000	0.000000	3.683184

Table A146: Cartesian coordinates in Angstroms (Å) for the C_{2v} optimized geometry of $Cl^{-}Ar_2$ at the MP2/QZ level of theory.

Atom	x	y	z
Cl	0.008223	0.000000	0.013960
Ar	0.006341	0.000000	3.686863
Ar	3.221529	0.000000	1.792972

Table A147: Cartesian coordinates in Angstroms (Å) for the $D_{\infty h}$ optimized geometry of $Cl^{-}Ar_2$ at the MP2/QZ level of theory.

Atom	x	y	z
Cl	0.000000	0.000000	0.000000
Ar	0.000000	0.000000	3.667768
Ar	0.000000	0.000000	−3.667768

Table A148: Cartesian coordinates in Angstroms (Å) for the C_{3v} optimized geometry of $Cl^{-}Ar_3$ at the MP2/QZ level of theory.

Atom	x	y	z
Cl	0.000000	0.000000	2.475144
Ar	0.000000	2.151291	−0.508649
Ar	−1.863073	−1.075645	−0.508649
Ar	1.863073	−1.075645	−0.508649

Table A149: Cartesian coordinates in Angstroms (Å) for the C_{2v} optimized geometry of $Cl^{-}Ar_3$ at the MP2/QZ level of theory.

Atom	x	y	z
Cl	0.000000	0.000000	−1.979832
Ar	0.000000	3.209813	−0.193129
Ar	0.000000	−3.209813	−0.193129
Ar	0.000000	0.000000	1.701377

Table A150: Cartesian coordinates in Angstroms (Å) for the C_{2v} optimized geometry of $Cl^{-}Ar_4$ at the MP2/QZ level of theory.

Atom	x	y	z
Cl	0.000000	0.000000	2.263015
Ar	0.000000	3.030420	0.177601
Ar	0.000000	−3.030420	0.177601
Ar	1.861689	0.000000	−0.917572
Ar	−1.861689	0.000000	−0.917572

Table A151: Cartesian coordinates in Angstroms (Å) for the T_d optimized geometry of Cl^-Ar_4 at the MP2/QZ level of theory.

Atom	x	y	z
Cl	0.000000	0.000000	0.000000
Ar	2.115632	2.115632	2.115632
Ar	−2.115632	−2.115632	2.115632
Ar	−2.115632	2.115632	−2.115632
Ar	2.115632	−2.115632	−2.115632

Table A152: Cartesian coordinates in Angstroms (Å) for the C_{4v} optimized geometry of Cl^-Ar_5 at the MP2/QZ level of theory.

Atom	x	y	z
Cl	0.000000	0.000000	−0.626846
Ar	0.000000	0.000000	3.172141
Ar	3.114795	0.000000	1.274940
Ar	0.000000	−3.114795	1.274940
Ar	−3.114795	0.000000	1.274940
Ar	0.000000	3.114795	1.274940

Table A153: Cartesian coordinates in Angstroms (Å) for the D_{3h} optimized geometry of $Cl^{-}Ar_5$ at the MP2/QZ level of theory.

Atom	x	y	z
Cl	0.000000	0.000000	0.000000
Ar	0.000000	0.000000	3.655625
Ar	3.165864	0.000000	−1.827813
Ar	−3.165864	0.000000	−1.827813
Ar	0.000000	3.652832	0.000000
Ar	0.000000	−3.652832	0.000000

Table A154: Cartesian coordinates in Angstroms (Å) for the C_{2v} optimized geometry of $Cl^{-}Ar_6$ at the MP2/QZ level of theory.

Atom	x	y	z
Cl	1.345052	0.988325	0.000000
Ar	−0.156764	−2.401505	0.000000
Ar	−2.338810	0.569164	0.000000
Ar	−0.325875	−0.239028	3.022781
Ar	3.513169	−1.970109	0.000000
Ar	−0.325875	−0.239028	−3.022781
Ar	−0.829474	3.942073	0.000000

Table A155: Cartesian coordinates in Angstroms (Å) for the O_h optimized geometry of Cl^-Ar_6 at the MP2/QZ level of theory.

Atom	x	y	z
Cl	0.000000	0.000000	0.000000
Ar	0.000000	0.000000	3.645893
Ar	0.000000	3.645893	0.000000
Ar	3.645893	0.000000	0.000000
Ar	0.000000	0.000000	−3.645893
Ar	0.000000	−3.645893	0.000000
Ar	−3.645893	0.000000	0.000000

Table A156: Cartesian coordinates in Angstroms (Å) for the $C_{\infty v}$ optimized geometry of Br^-Ar at the MP2/QZ level of theory.

Atom	x	y	z
Br	0.000000	0.000000	0.000000
Ar	0.000000	0.000000	3.870597

Table A157: Cartesian coordinates in Angstroms (Å) for the C_{2v} optimized geometry of Br^-Ar_2 at the MP2/QZ level of theory.

Atom	x	y	z
Br	0.000000	0.000000	0.000000
Ar	0.000000	0.000000	3.875837
Ar	3.271673	0.000000	2.078045

Table A158: Cartesian coordinates in Angstroms (Å) for the $D_{\infty h}$ optimized geometry of $Br^{-}Ar_2$ at the MP2/QZ level of theory.

Atom	x	y	z
Br	0.000000	0.000000	0.000000
Ar	0.000000	0.000000	3.871699
Ar	0.000000	0.000000	−3.871699

Table A159: Cartesian coordinates in Angstroms (Å) for the C_{3v} optimized geometry of $Br^{-}Ar_3$ at the MP2/QZ level of theory.

Atom	x	y	z
Br	0.000000	0.000000	1.958817
Ar	0.000000	2.152313	−1.269604
Ar	−1.863959	−1.076157	−1.269604
Ar	1.863958	−1.076157	−1.269604

Table A160: Cartesian coordinates in Angstroms (Å) for the C_{2v} optimized geometry of $Br^{-}Ar_3$ at the MP2/QZ level of theory.

Atom	x	y	z
Br	0.000000	0.000000	1.628757
Ar	0.000000	3.266720	−0.456368
Ar	0.000000	−3.266720	−0.456368
Ar	0.000000	0.000000	−2.254291

Table A161: Cartesian coordinates in Angstroms (Å) for the C_{2v} optimized geometry of $Br^{-}Ar_4$ at the MP2/QZ level of theory.

Atom	x	y	z
Br	0.000000	0.000000	1.950884
Ar	0.000000	3.057216	−0.437339
Ar	0.000000	−3.057216	−0.437339
Ar	1.862839	0.000000	−1.459355
Ar	−1.862839	0.000000	−1.459355

Table A162: Cartesian coordinates in Angstroms (Å) for the T_d optimized geometry of $Br^{-}Ar_4$ at the MP2/QZ level of theory.

Atom	x	y	z
Br	0.000000	0.000000	0.000000
Ar	2.232513	2.232513	2.232513
Ar	−2.232513	−2.232513	2.232513
Ar	−2.232513	2.232513	−2.232513
Ar	2.232513	−2.232513	−2.232513

Table A163: Cartesian coordinates in Angstroms (Å) for the C_{4v} optimized geometry of Br^-Ar_5 at the MP2/QZ level of theory.

Atom	x	y	z
Br	0.000000	0.000000	0.000000
Ar	0.000000	0.000000	4.022783
Ar	3.157868	0.000000	2.196570
Ar	0.000000	−3.157868	2.196570
Ar	−3.157868	0.000000	2.196570
Ar	0.000000	3.157868	2.196570

Table A164: Cartesian coordinates in Angstroms (Å) for the D_{3h} optimized geometry of Br^-Ar_5 at the MP2/QZ level of theory.

Atom	x	y	z
Br	0.000000	0.000000	0.000000
Ar	0.000000	0.000000	3.858816
Ar	3.341832	0.000000	−1.929408
Ar	−3.341832	0.000000	−1.929408
Ar	0.000000	3.857057	0.000000
Ar	0.000000	−3.857057	0.000000

Table A165: Cartesian coordinates in Angstroms (Å) for the C_{2v} optimized geometry of $Br^{-}Ar_6$ at the MP2/QZ level of theory.

Atom	x	y	z
Br	−1.376327	−0.737714	0.000000
Ar	0.788693	2.516045	0.000000
Ar	2.531990	−0.736395	0.000000
Ar	0.718191	0.384898	3.048357
Ar	−2.896883	2.819339	0.000000
Ar	0.718191	0.384898	−3.048357
Ar	0.743620	−3.973424	0.000000

Table A166: Cartesian coordinates in Angstroms (Å) for the O_h optimized geometry of $Br^{-}Ar_6$ at the MP2/QZ level of theory.

Atom	x	y	z
Br	0.000000	0.000000	0.000000
Ar	0.000000	0.000000	3.850819
Ar	0.000000	3.850819	0.000000
Ar	3.850819	0.000000	0.000000
Ar	0.000000	0.000000	−3.850819
Ar	0.000000	−3.850819	0.000000
Ar	−3.850819	0.000000	0.000000

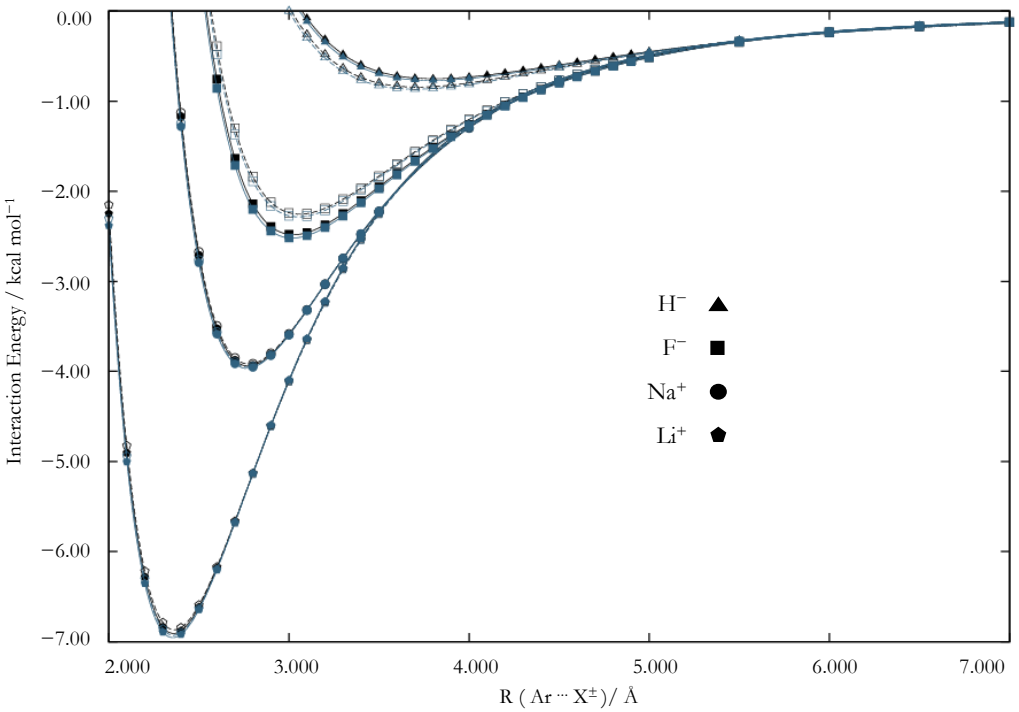

Figure A1: M^+Ar_1 and X^-Ar_1 interatomic distance scan for various ions. Shaded markers indicate CCSD(T) values, where empty markers indicate MP2 values. Black lines indicate QZ values, where blue lines indicate 5Z values.

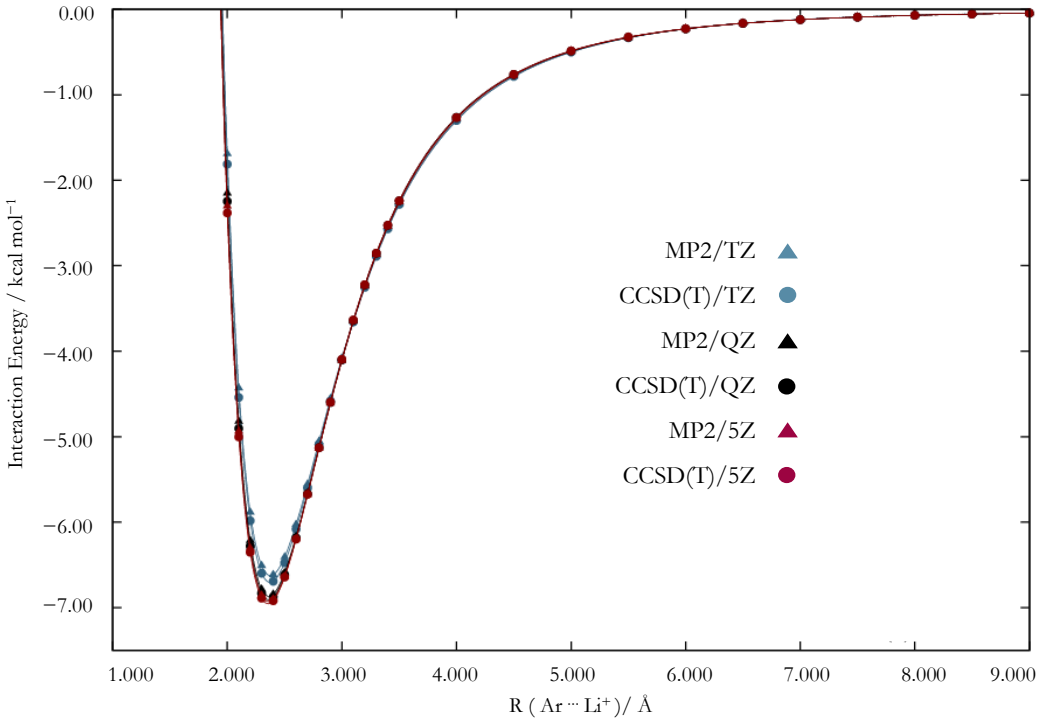

Figure A2: Li^+Ar_1 interatomic distance scan at the MP2/XZ and CCSD(T)/XZ (X = T, Q, and 5) level of theory.

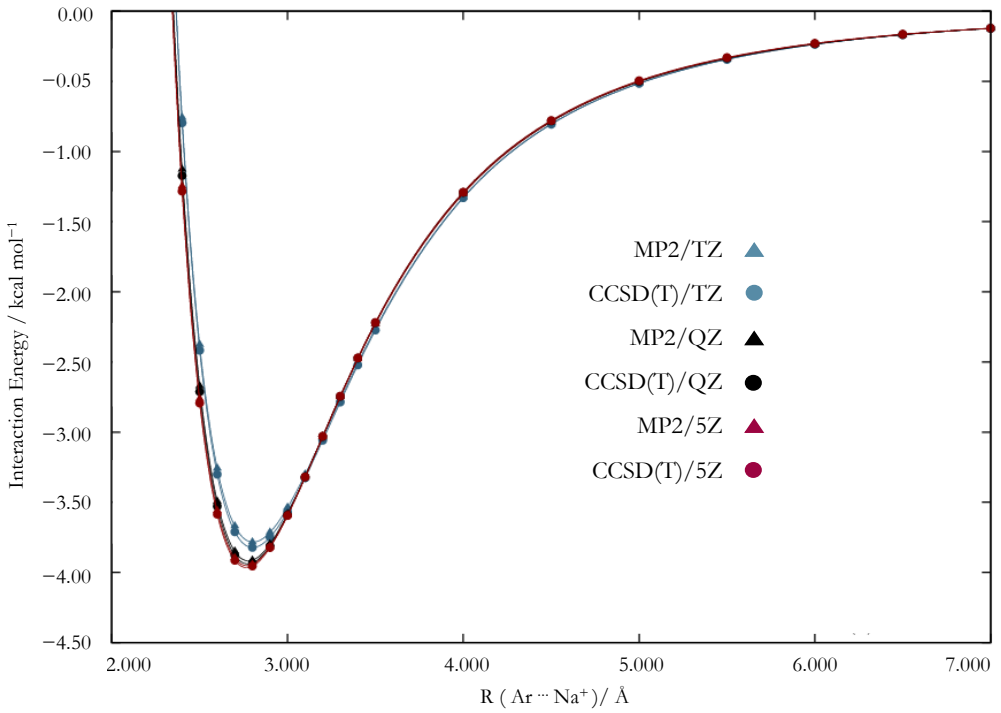

Figure A3: Na^+Ar_1 interatomic distance scan at the MP2/XZ and CCSD(T)/XZ (X = T, Q, and 5) level of theory.

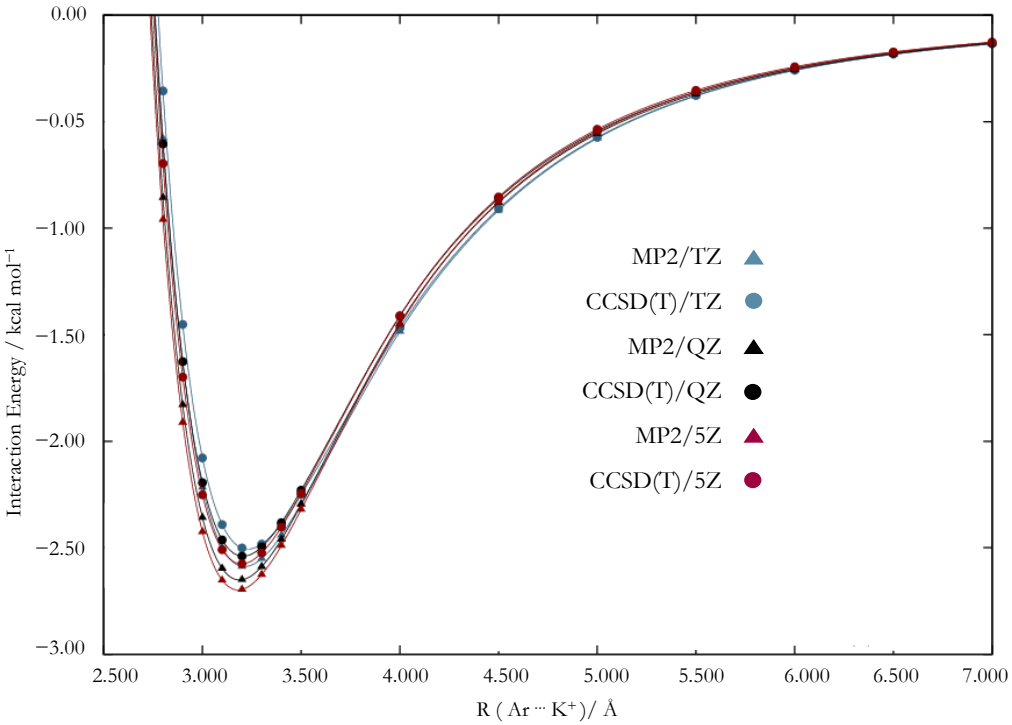

Figure A4: K^+Ar_1 interatomic distance scan at the MP2/XZ and CCSD(T)/XZ (X = T, Q, and 5) level of theory.

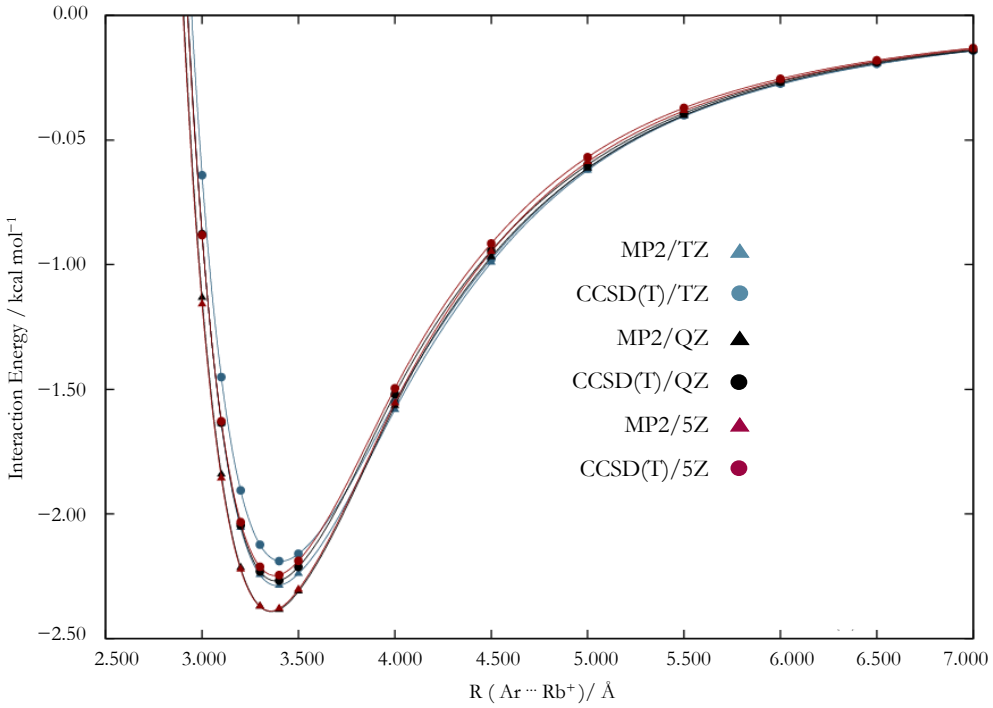

Figure A5: Rb^+Ar_1 interatomic distance scan at the MP2/XZ and CCSD(T)/XZ (X = T, Q, and 5) level of theory.

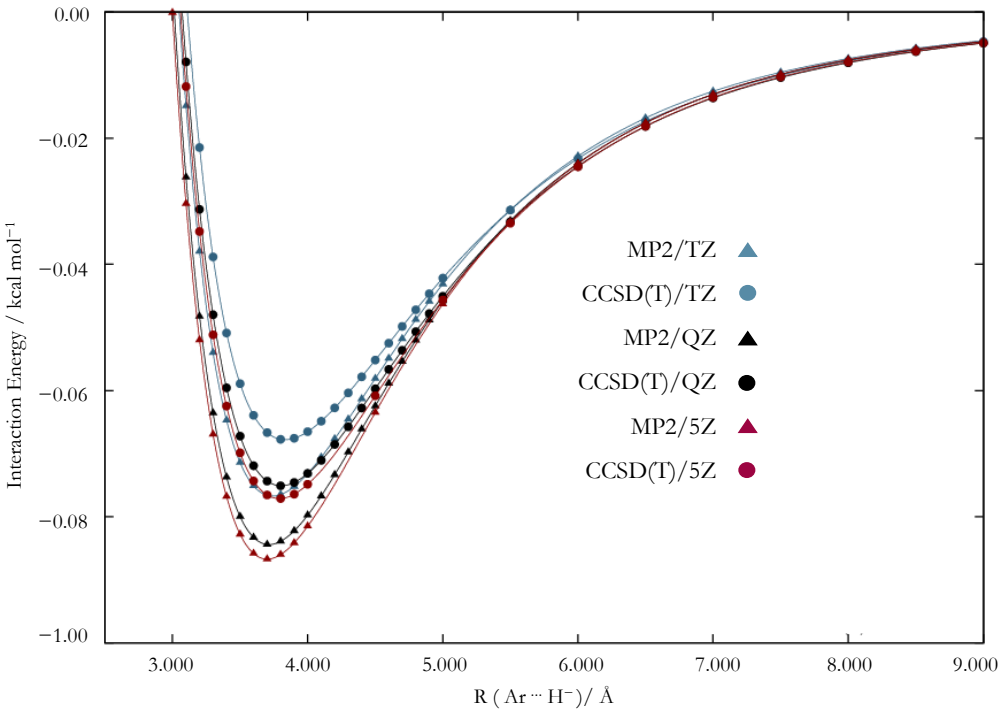

Figure A6: $H^{-}Ar_1$ interatomic distance scan at the MP2/XZ and CCSD(T)/XZ (X = T, Q, and 5) level of theory.

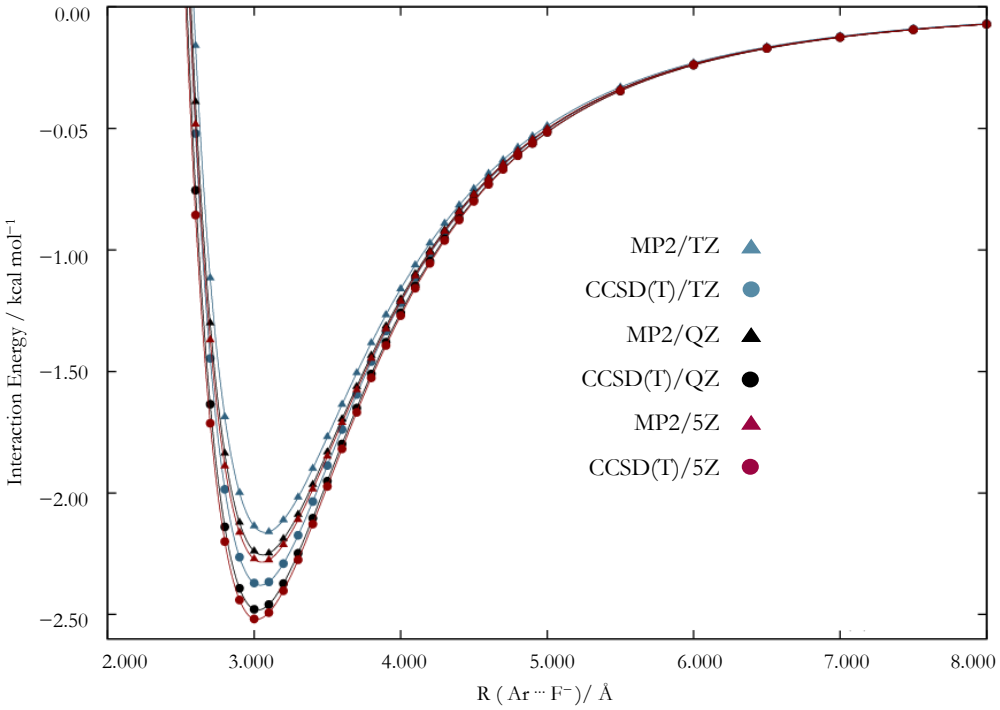

Figure A7: $F^{-}Ar_1$ interatomic distance scan at the MP2/XZ and CCSD(T)/XZ (X = T, Q, and 5) level of theory.

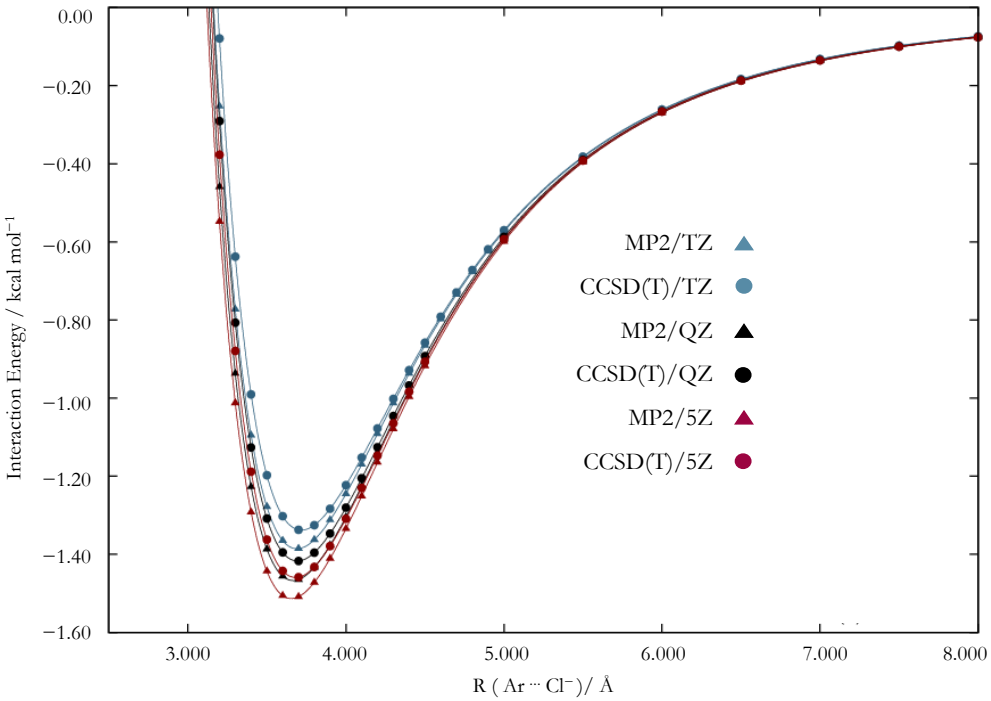

Figure A8: $Cl^{-}Ar_1$ interatomic distance scan at the MP2/XZ and CCSD(T)/XZ (X = T, Q, and 5) level of theory.

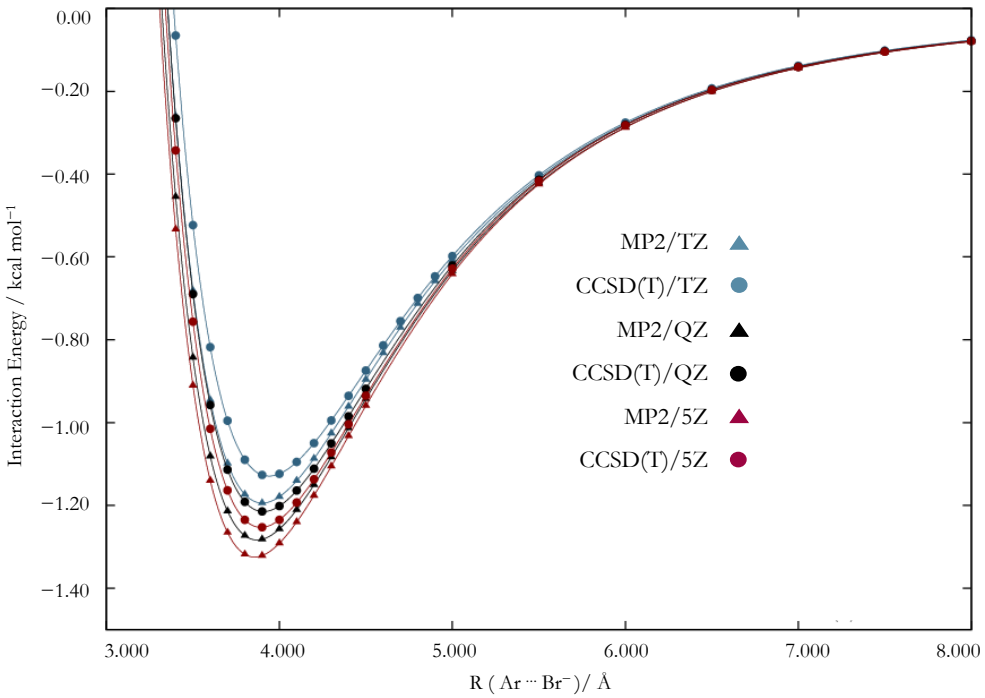

Figure A9: $Br^{-}Ar_1$ interatomic distance scan at the MP2/XZ and CCSD(T)/XZ (X = T, Q, and 5) level of theory.

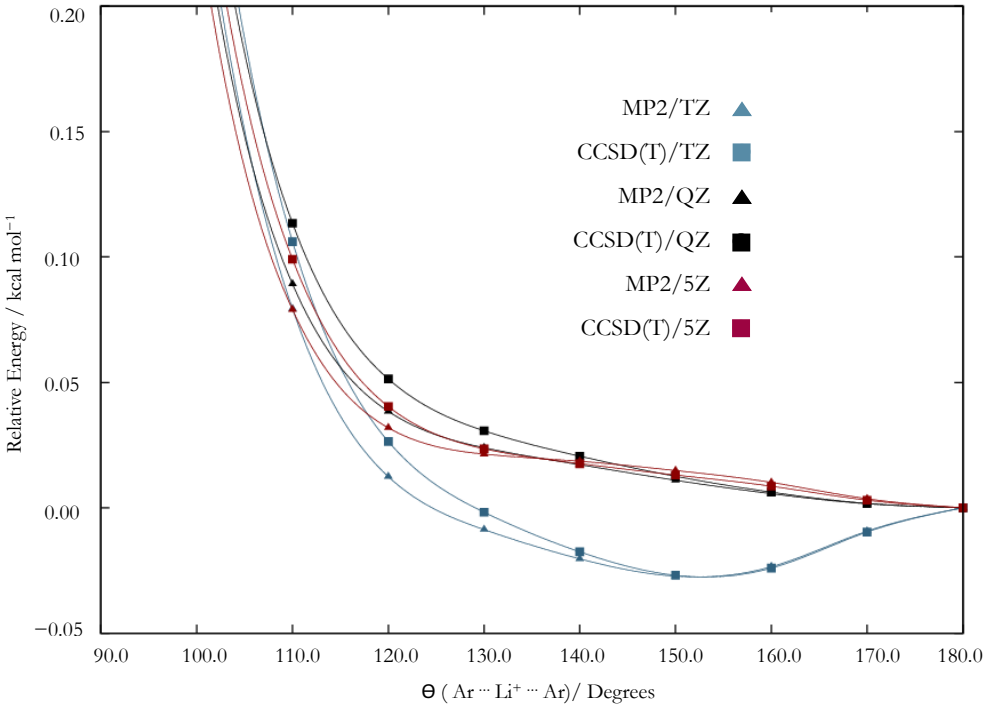

Figure A10: Li^+Ar_2 relaxed angular scan at the MP2/XZ and CCSD(T)/XZ (X = T, Q, and 5) level of theory.

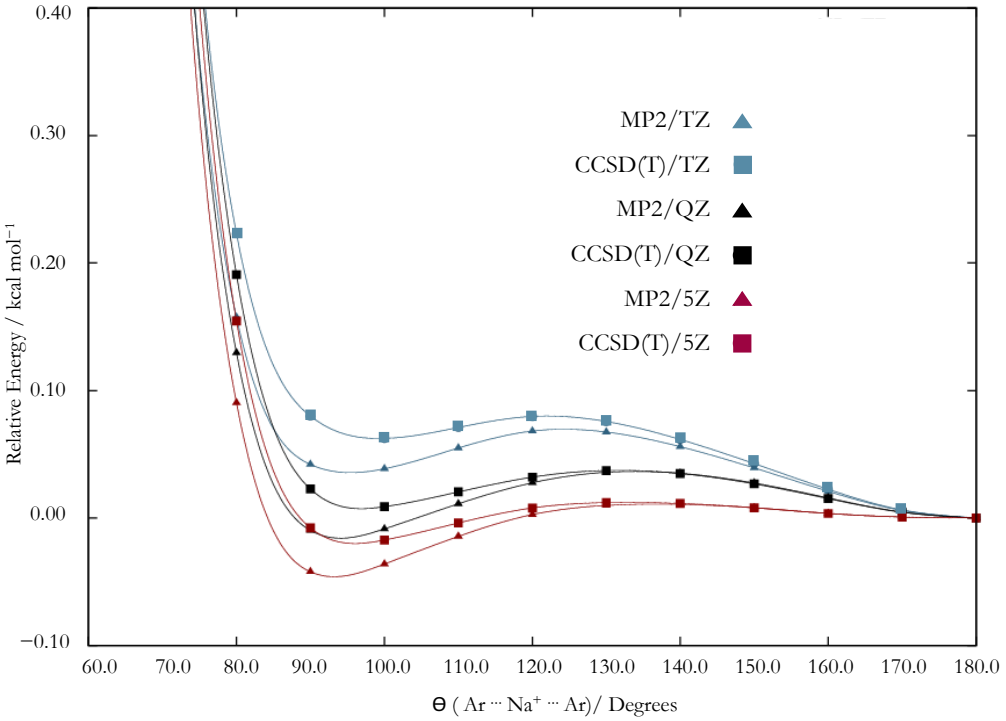

Figure A11: Na^+Ar_2 relaxed angular scan at the MP2/XZ and CCSD(T)/XZ (X = T, Q, and 5) level of theory.

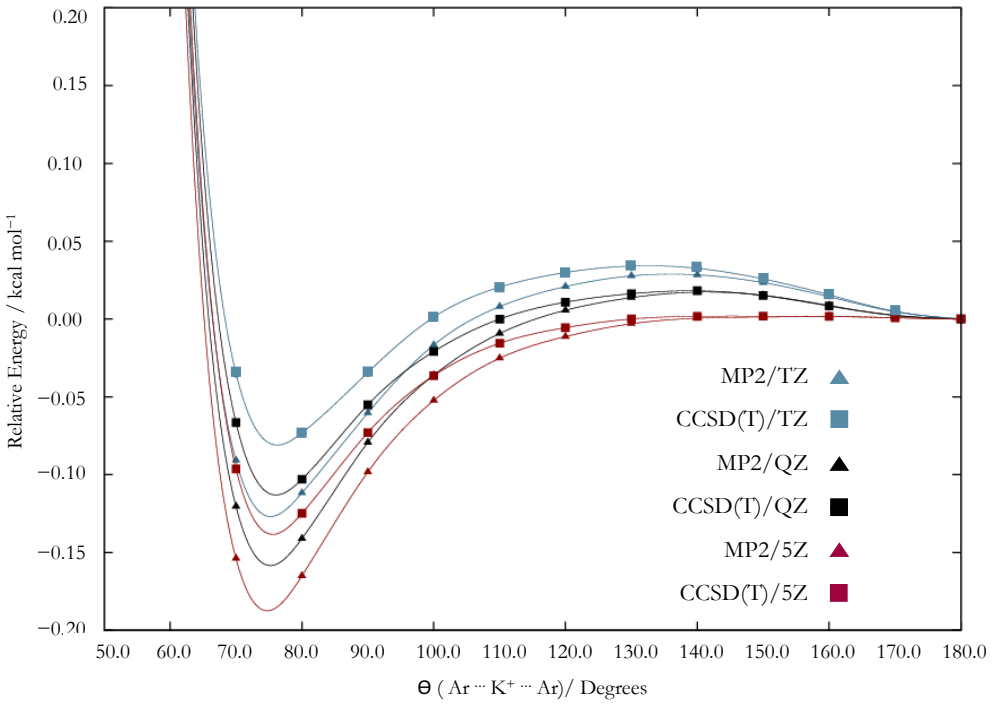

Figure A12: K^+Ar_2 relaxed angular scan at the MP2/XZ and CCSD(T)/XZ (X = T, Q, and 5) level of theory.

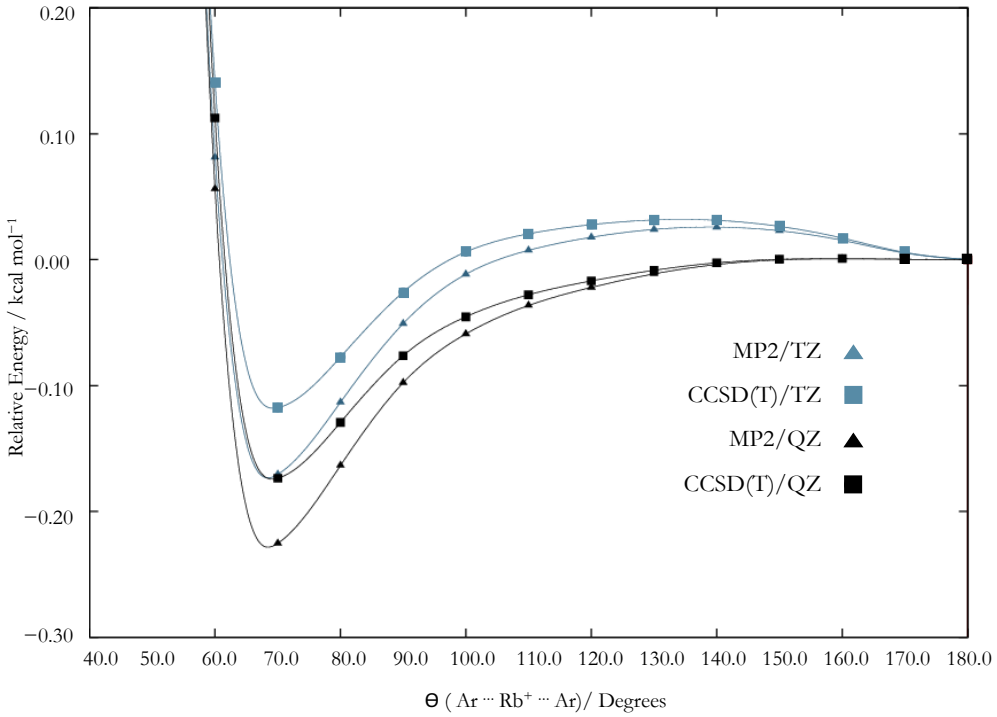

Figure A13: Rb^+Ar_2 relaxed angular scan at the MP2/XZ and CCSD(T)/XZ (X = T and Q) level of theory.

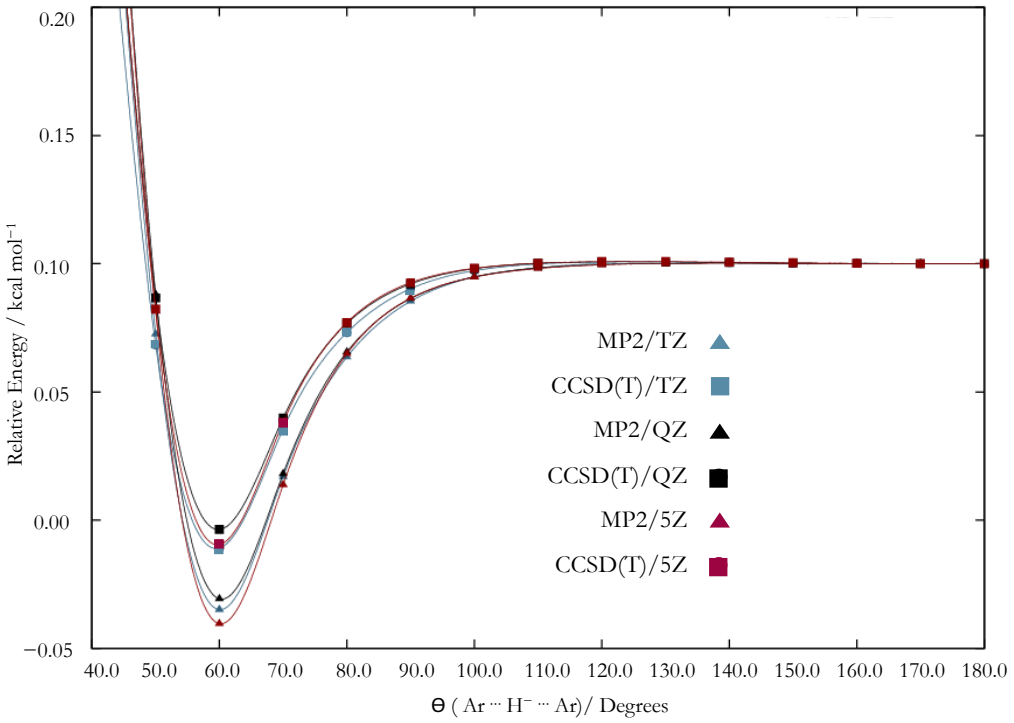

Figure A14: H^-Ar_2 relaxed angular scan at the MP2/XZ and CCSD(T)/XZ (X = T, Q, and 5) level of theory.

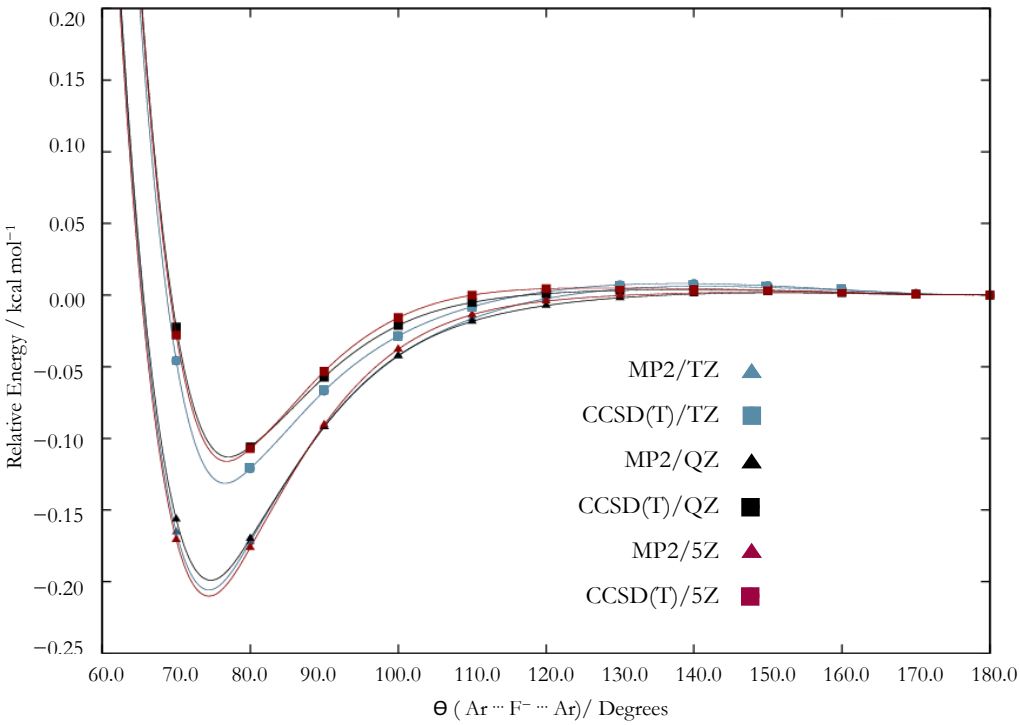

Figure A15: $F^{-}Ar_2$ relaxed angular scan at the MP2/XZ and CCSD(T)/XZ (X = T, Q, and 5) level of theory.

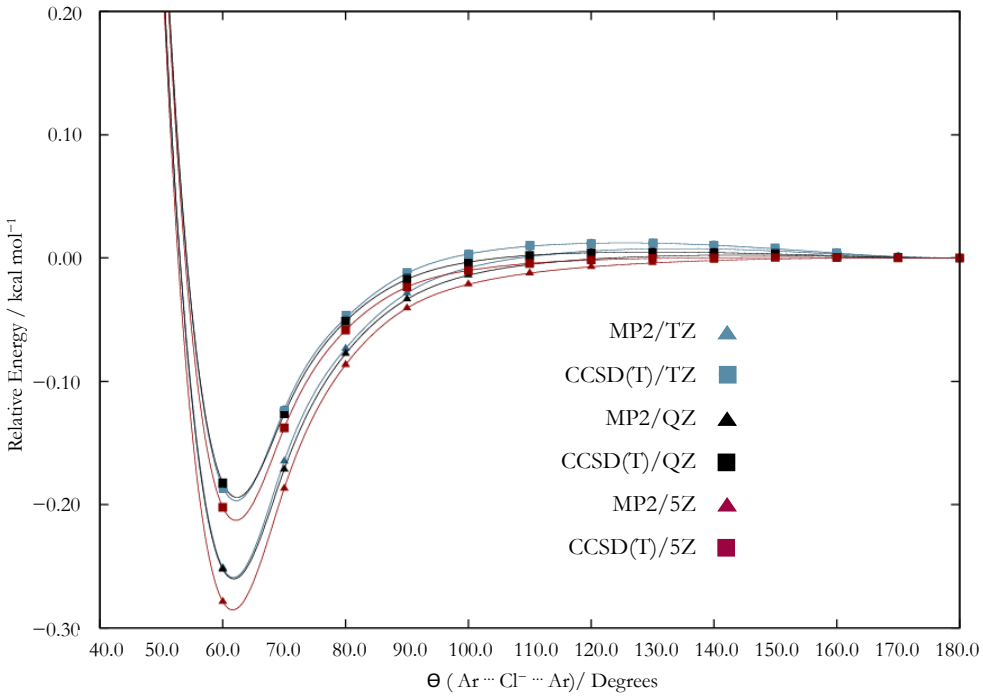

Figure A16: $Cl^{-}Ar_2$ relaxed angular scan at the MP2/XZ and CCSD(T)/XZ (X = T, Q, and 5) level of theory.

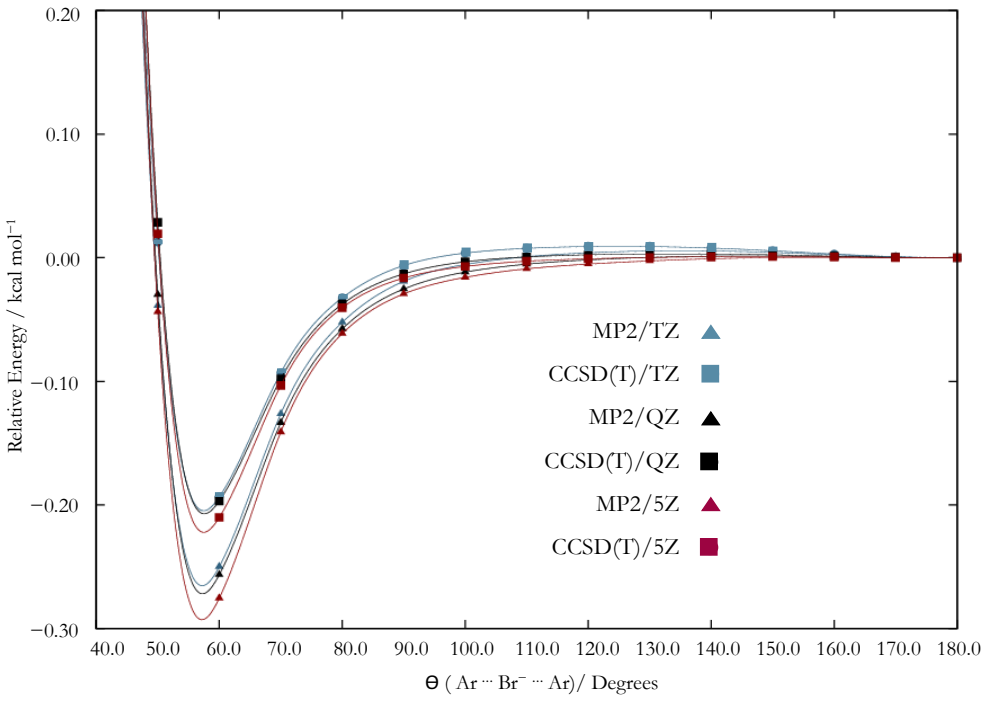

Figure A17: $Br^{-}Ar_2$ relaxed angular scan at the MP2/XZ and CCSD(T)/XZ (X = T, Q, and 5) level of theory.

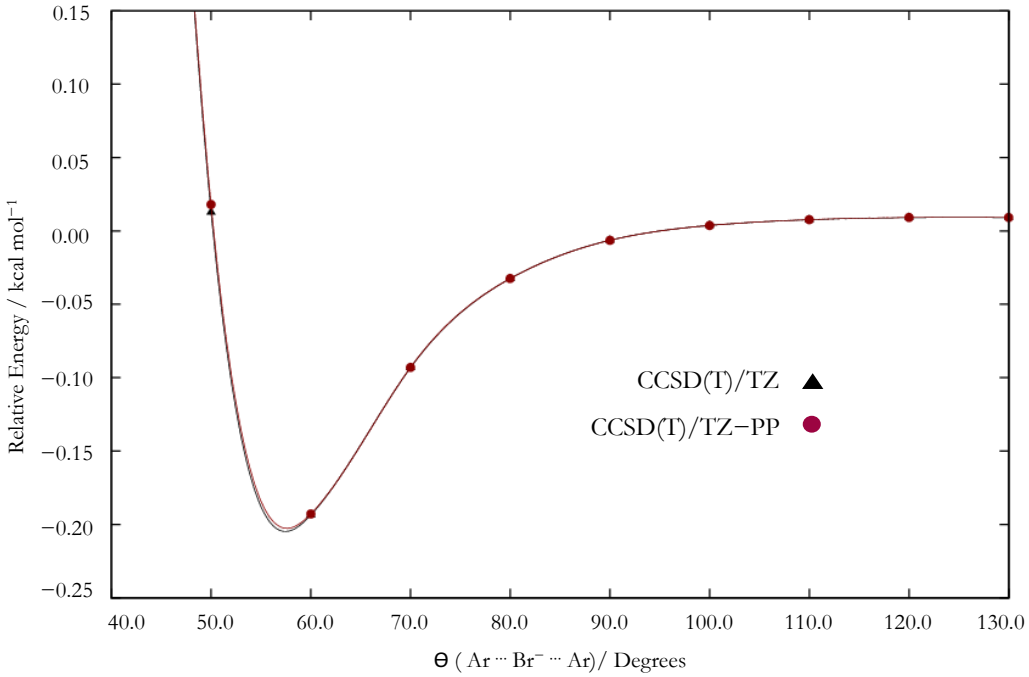

Figure A18: $Br^{-}Ar_2$ relaxed angular scan at the MP2/TZ and CCSD(T)/TZ level of theory. Red indicates the use of a pseudopotential.

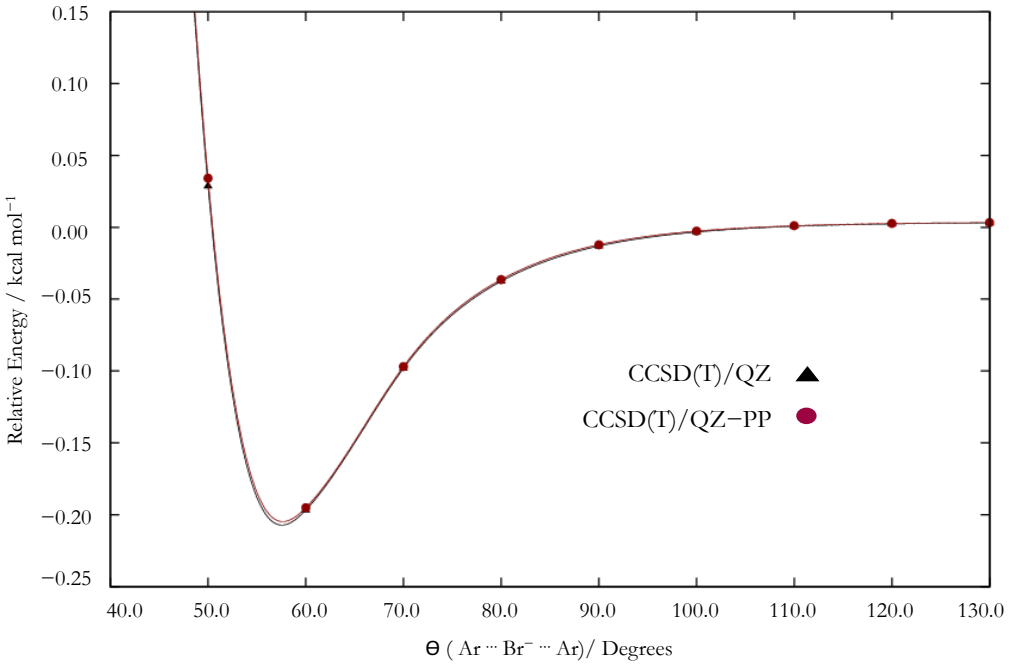

Figure A19: $Br^{-}Ar_2$ relaxed angular scan at the MP2/QZ and CCSD(T)/QZ level of theory. Red indicates the use of a pseudopotential.

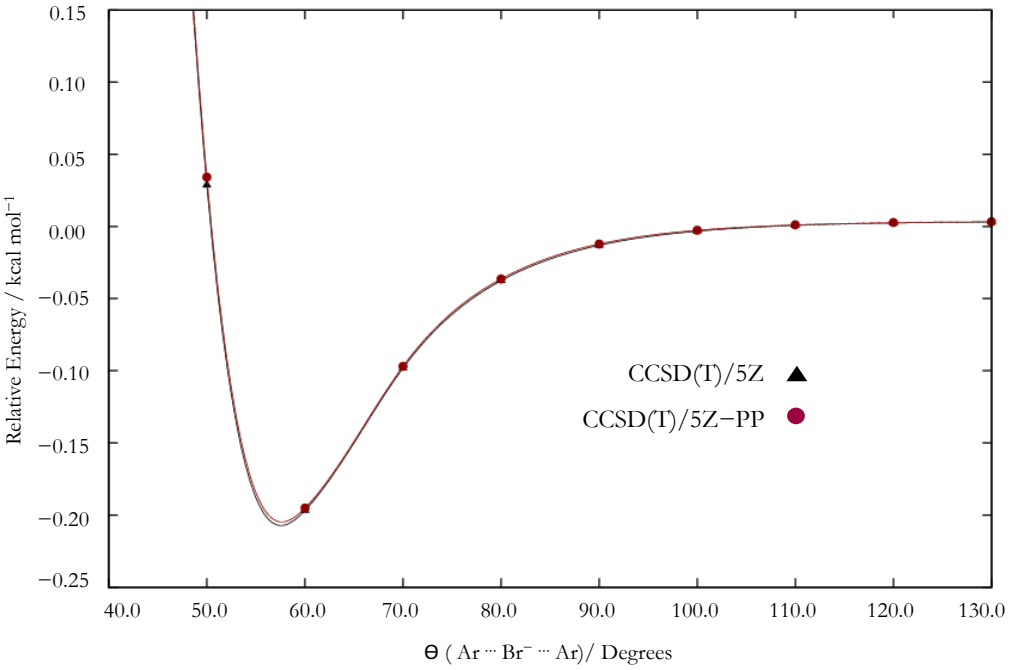

Figure A20: $Br^{-}Ar_2$ relaxed angular scan at the MP2/5Z and CCSD(T)/5Z level of theory. Red indicates the use of a pseudopotential.